Article

Developmental Cell

A Quick HYL1-Dependent Reactivation of MicroRNA Production Is Required for a Proper Developmental Response after Extended Periods of Light Deprivation

Graphical Abstract

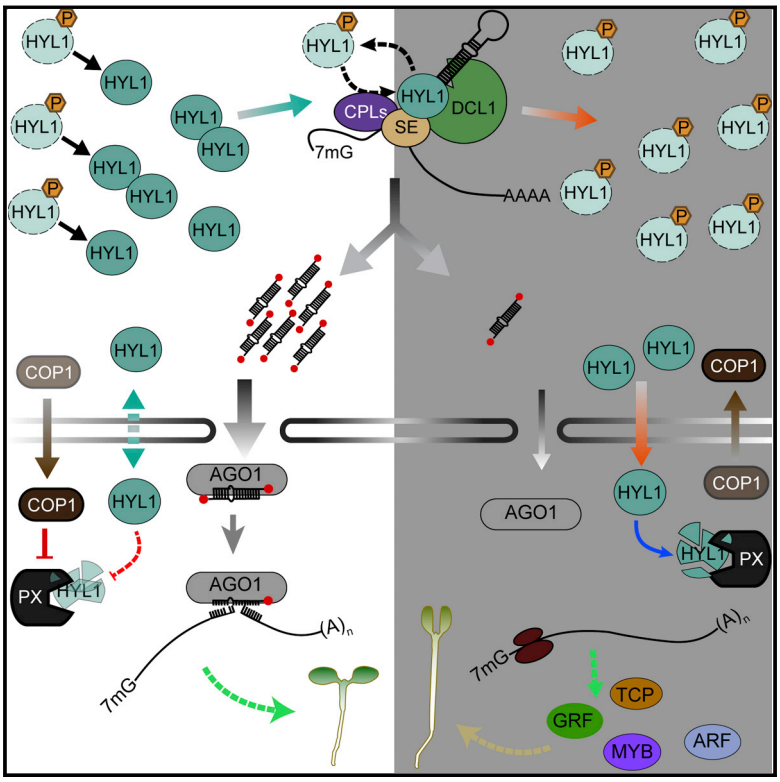

Highlights

- Phosphorylated miRNA biogenesis factor HYL1 forms a nuclear reserve of inactive protein
- Light-dependent dephosphorylation of the reserve pool restores miRNA production
- Nuclear retention of phosphorylated HYL1 protects it from dark-induced degradation
- HYL1 homeostasis affects plant developmental response to light availability

Authors

Natalia P. Achkar, Seok Keun Cho, Christian Poulsen, ..., Jorge J. Casal, Seong Wook Yang, Pablo A. Manavella

Correspondence

yangsw@yonsei.ac.kr (S.W.Y.), pablomanavella@ial.santafe-conicet.gov.ar (P.A.M.)

In Brief

Achkar et al. show that a nuclear reserve pool of inactive phosphorylated HYL1, an essential cofactor for microRNA biogenesis, is resistant to dark- or shade-induced degradation. Upon light restoration, this HYL1 pool is quickly dephosphorylated to rapidly restore miRNA production and switch the developmental program to light-dependent growth.

Achkar et al., 2018, Developmental Cell *46*, 236–247
July 16, 2018
https://doi.org/10.1016/j.devcel.2018.06.014

CellPress

CellPress

Developmental Cell
Article

A Quick HYL1-Dependent Reactivation of MicroRNA Production Is Required for a Proper Developmental Response after Extended Periods of Light Deprivation

Natalia P. Achkar,[1,7] Seok Keun Cho,[2,7] Christian Poulsen,[4,7] Agustin L. Arce,[1] Delfina A. Re,[1] Axel J. Giudicatti,[1] Elizabeth Karayekov,[3] Moon Young Ryu,[2] Suk Won Choi,[2] Jesper Harholt,[4] Jorge J. Casal,[3,5] Seong Wook Yang,[2,6,*] and Pablo A. Manavella[1,8,*]

[1]Instituto de Agrobiotecnología del Litoral (CONICET-UNL-FBCB), Santa Fe 3000, Argentina
[2]Department of Systems Biology, College of Life Science and Biotechnology, Yonsei University, Seoul, Korea
[3]IFEVA, Facultad de Agronomía, Universidad de Buenos Aires, Buenos Aires 1417, Argentina
[4]Carlsberg Research Laboratory, Copenhagen V 1799, Denmark
[5]Fundación Instituto Leloir, Instituto de Investigaciones Bioquímicas de Buenos Aires-CONICET, Buenos Aires 1405, Argentina
[6]Department of Plant and Environmental Science, Faculty of Science, University of Copenhagen, Copenhagen, Denmark
[7]These authors contributed equally
[8]Lead Contact
*Correspondence: yangsw@yonsei.ac.kr (S.W.Y.), pablomanavella@ial.santafe-conicet.gov.ar (P.A.M.)
https://doi.org/10.1016/j.devcel.2018.06.014

SUMMARY

Light is the most influential environmental stimulus for plant growth. In response to deficient light, plants reprogram their development to adjust their growth in search for a light source. A fine reprogramming of gene expression orchestrates this adaptive trait. Here we show that plants alter microRNA (miRNA) biogenesis in response to light transition. When plants suffer an unusual extended period of light deprivation, the miRNA biogenesis factor HYPONASTIC LEAVES 1 (HYL1) is degraded but an inactive pool of phosphorylated protein remains stable inside the nucleus. Degradation of HYL1 leads to the release of gene silencing, triggering a proper response to dark and shade. Upon light restoration, a quick dephosphorylation of HYL1 leads to the reactivation of miRNA biogenesis and a switch toward a developmental program that maximizes the light uptake. Our findings define a unique and fast regulatory mechanism controlling the plant silencing machinery during plant light response.

INTRODUCTION

As photo-autotrophic organisms, plants depend on light, a resource that may become temporarily limiting. For instance, plants are inevitably exposed to darkness during the night. In addition, plants can eventually experience limited light for much longer periods (days) when seeds germinate underground, when soil disturbance causes reburial of aerial organs, and when neighboring plants overtop their foliage. These fluctuations can challenge plant survival. Plants repress the photomorphogenic program switching to skotomorphogenesis in response to prolonged darkness. Furthermore, in response to the presence of neighbors, plants initiate shade avoidance responses. Skotomorphogenesis and shade avoidance tend to overcome the light limitation; for instance, by enhancing stem extension to push their foliage out of either the soil or the shade of neighbors (Ballare and Pierik, 2017; Seluzicki et al., 2017; Wu, 2014). Upon light restoration, the termination of skotomorphogenesis (also known as de-etiolation) or shade avoidance is characterized by the reversal of the above changes in favor of an enhanced photosynthetic capacity. Such developmental plasticity is orchestrated at the transcriptional level by the harmonious temporal and spatial expression of specific transcription factors (Wu, 2014). Post-transcriptional gene silencing mediated by microRNAs (miRNAs) and *trans*-acting small interfering RNAs (ta-siRNAs) are necessary to balance many developmental processes, including growth (Li et al., 2017).

In the model plant *Arabidopsis thaliana*, the biogenesis of miRNAs begins with the transcription of a miRNA gene by the RNA polymerase II. The generated transcript (pri-miRNA) suffers successive cuts until a mature double-stranded miRNA is released. The mature miRNA duplex is then loaded into one of the 10 *Arabidopsis* Argonaute (AGO) proteins and guides the silencing of target mRNAs (Rogers and Chen, 2013). The miRNA processing complex comprises the RNase III endonuclease Dicer-like 1 (DCL1); the RNA binding protein HYPONASTIC LEAVES 1 (HYL1), known also as DRB1 and functionally homologous to animal DGCR8 and TRBP; and the zinc finger protein SERRATE (SE), among others (Achkar et al., 2016). Within this complex, DCL1 is the enzyme responsible for converting the pri-miRNA into the miRNA:miRNA* duplex (Kurihara and Watanabe, 2004). HYL1 and SE are largely known to assist DCL1 in finding the precise cutting site to excise an active miRNA (Dong et al., 2008; Kurihara et al., 2006). The maintenance of steady-state levels of functional miRNAs ensures a normal plant homeostasis and any fluctuation in the miRNA production will affect a cascade of downstream processes (Meng et al., 2011).

In plants, the regulation of the miRNA biogenesis is not an unusual phenomenon to modify the mature miRNAs population in a given tissue or condition (Achkar et al., 2016; Reis et al., 2015).

As with its homologs in humans, HYL1 is a heavily regulated component of the miRNA pathway. This protein is composed of two double-stranded RNA binding motifs (DRBMs); DRBM1, responsible for the interaction of HYL1 with pri-miRNAs, and DRBM2, which enables protein-protein interactions (Yang et al., 2010). HYL1 activity is post-translationally regulated by phosphorylation. C-TERMINAL DOMAIN PHOSPHATASE-LIKE 1 and 2 (CPL1 and CPL2) and the Protein Phosphatase 4 (PP4)/Suppressor of MEK 1 (SMEK1) complex dephosphorylate HYL1 to enhance its activity (Manavella et al., 2012; Su et al., 2017). On the other hand, SnRK2 and MPK3 kinases were proposed to trigger HYL1 phosphorylation (Raghuram et al., 2015; Yan et al., 2017). Specifically, two serine residues, S42 and S159, localized in DRBM1 and DRBM2 respectively, are particularly important for this regulation (Karlsson et al., 2015; Manavella et al., 2012). Additionally, HYL1 protein levels are modulated by light conditions. In the dark, HYL1 is degraded, while in the light the E3 ubiquitin ligase CONSTITUTIVE PHOTOMORPHOGENIC 1 (COP1) prevents its degradation (Cho et al., 2014). Despite HYL1 activity, and therefore miRNA production, being post-translationally regulated, it is unclear if such regulation has any physiological relevance for plant homeostasis. Based on this, we define the non-phosphorylated isoform, which is able to act during miRNA biogenesis, as active HYL1 and the phosphorylated version as inactive. This definition does not exclude a potential function of phosphorylated HYL1.

Here, we report that, under prolonged shade or darkness, the exclusive nuclear localization of phosphorylated HYL1 protects it from proteolytic degradation and allows the formation of an inactive protein reserve pool under periods of limited light. Upon light restoration, this inactive HYL1 reserve pool is quickly dephosphorylated to reactivate miRNA production. We found that the dynamic conversion between these HYL1 isoforms is essential to adjust plant development to the prevailing conditions. Both the degradation of the active HYL1 form during prolonged periods of darkness or shade as well as the presence of the phosphorylated reserve pool are necessary to support the adaptive developmental responses. This phenomenon is only triggered when the period of dark or shade extends longer than a normal day-night oscillation. Genome-wide, this degradation/reactivation of HYL1 produces an extensive change in the miRNA production and the regulation of specific transcription factors to control plant growth in response to darkness/shade or light. Remarkably, the quick nature of the HYL1 reactivation mechanism provides one of the few examples where post-translational regulation of a central player in miRNA biogenesis mediates a fast switch between opposite developmental responses.

RESULTS

Prolonged Periods of Darkness or Shade Strongly Increase the Ratio between Phosphorylated and Dephosphorylated HYL1

Since miRNA production depends on the balance between dephosphorylated (active) and phosphorylated (inactive) HYL1, we investigated the steady levels of the HYL1 isoforms in different plant organs, in response to exogenous applications of hormones and as a result of different light and temperature conditions. We separated the HYL1 phosphoisoforms by using Phos-tag polyacrylamide gels and calculated the phosphorylated/non-phosphorylated ratio, which can be compared among the different samples despite differences in total HYL1 abundance. The results showed that the ratio increases with increasing age in seedlings (5–7 versus 12 days old), in rosette leaves (emerging versus fully expanded) and flower buds (closed versus open) (Figure 1A). In 10-day-old seedlings, exposure to low temperature, jasmonic acid, auxin, gibberellins, or cytokinin caused negligible effects on the isoform balance. However, the ethylene precursor ACC and the phytohormone ABA produced a shift in the HYL1 isoforms ratio toward the phosphorylated (inactive) form (Figure 1B). The change caused by ABA is particularly interesting considering that *hyl1* mutant plants are hypersensitive to this hormone (Lu and Fedoroff, 2000). However, the largest shift in isoforms ratio was observed when plants were exposed to prolonged periods of deficient light. For instance, a high proportion of the inactive form of HYL1 was observed in plants transferred from light to darkness for 3–4 days to simulate reburial, in etiolated seedlings grown in full darkness after seed germination to initiate skotomorphogenesis, in seedlings exposed to weak unilateral blue light (which does not fully revert de-etiolation), and in seedlings transferred from light to simulated shade from neighbors (Figures 1B and 1C). Since the photosynthetic pigments of leaves absorb visible light much more than far-red light, we used a selective filter that severely reduced visible light but transmitted most of the far-red to simulate canopy shade. As expected from previous reports (Cho et al., 2014), the tested light conditions caused a reduction in HYL1 levels, without a change in *HYL1* transcript levels or SE levels (Figures S1A and S1B). Concomitant with a HYL1 reduction (Figures S1C and S1D), the levels of miRNAs decreased gradually during prolonged shade or darkness and recovered quickly after the return to white light (Figures S1E and S1F). No significant differences were observed for miR168, which is commonly independent of HYL1-mediated processing (Eamens et al., 2009) and used here as a control of a HYL1-independent pathway. During a simulated light/dark daily cycle, HYL1 remained stable during the first 8 hr of the night and gradually decreased afterward, recovering its abundance in the first hours of light (Figure S1G). However, contrary to the effects of prolonged darkness or shade, the transient HYL1 decrease observed at the end of the night did not result in detectable changes in miRNA levels (Figure S1H).

The Inactive Phosphorylated HYL1 Is Less Susceptible to Dark- or Shade-Induced Degradation and Forms a Protein Reserve Pool

The observed increase in phosphorylated/dephosphorylated HYL1 ratio in response to darkness or shade could be explained by a change in HYL1 phosphorylation and/or selective degradation of the dephosphorylated form. To distinguish between these possibilities, we used Phos-tag acrylamide gels to separate the HYL1 isoform in the same samples used in Figures S1C and S1D. When HYL1 isoforms were evaluated individually we observed that only the non-phosphorylated HYL1 form was degraded, both in dark and shade (Figure 1D). The reduction of the total amount of HYL1, with relatively stable levels of phosphorylated HYL1, suggests that HYL1 degradation proceeded mainly from the dephosphorylated HYL1 form (almost

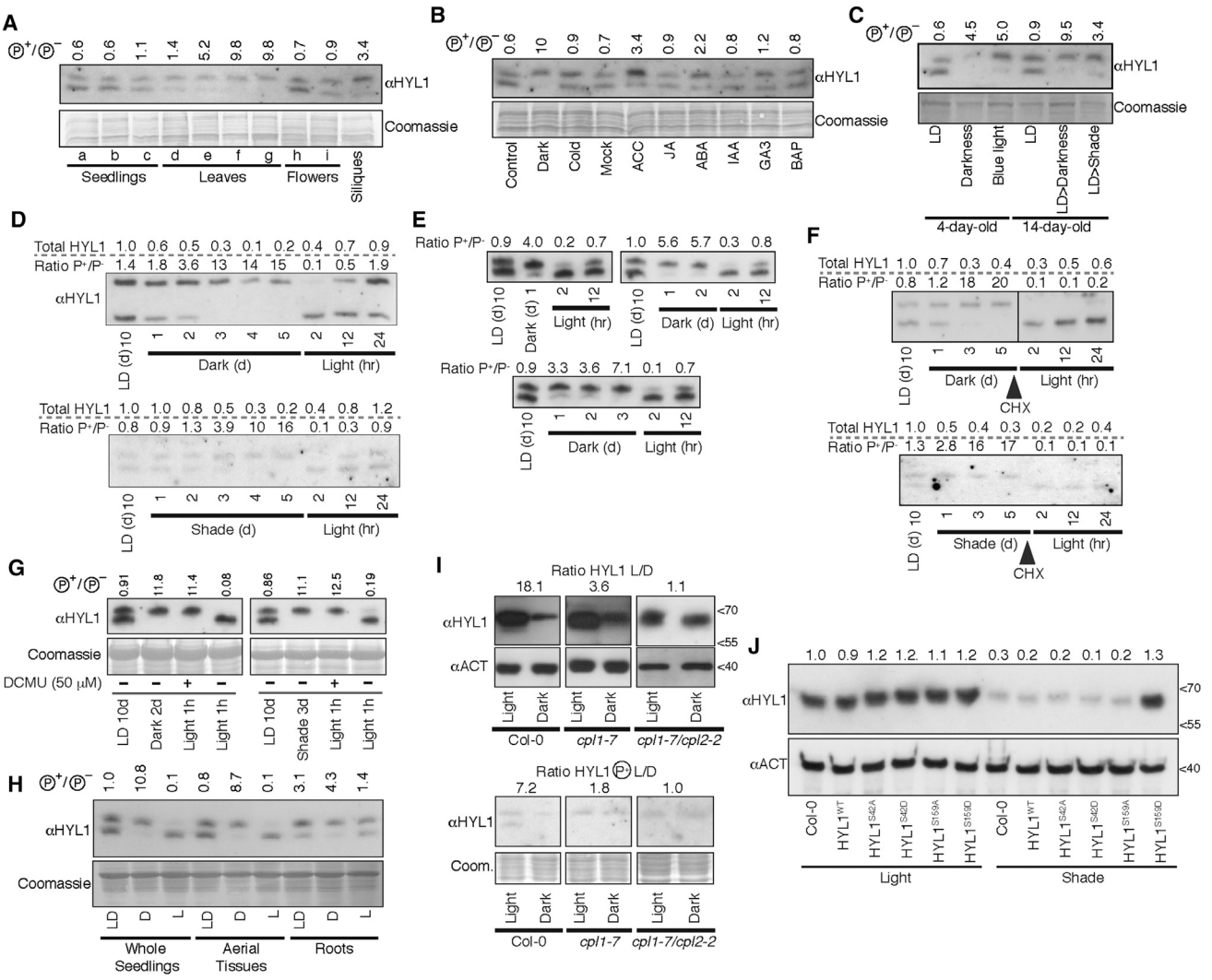

Figure 1. Phosphorylated HYL1 Is Resistant to Degradation Accumulating as a Reserve Pool during Prolonged Darkness

(A–C) Phosphoprotein mobility shift gels probed with anti-HYL1 antibody (upper panels). Bottom panels show Coomassie stain as loading control. Ratios between the phosphorylated and non-phosphorylated HYL1 forms are given at the top of each band pair. Loaded samples correspond to (A) whole seedlings collected 5, 7, and 12 days after germination (a, b, and c respectively); emerging, developing, fully expanded, and cauline leaves (d, e, f, and g respectively); close and open floral buds (h and i respectively); and fully expanded siliques. (C) Samples collected 4 days after germination under long-day (LD) photoperiod, complete darkness (Darkness) or with a faint localized light source (Blue light). LD-grown 10-day-old seedlings transferred to LD photoperiod, complete darkness (LD>Darkness), or a green light source (LD > Shade) for 4 days.

(D–F) Phosphoprotein mobility shift gels probed with anti-HYL1 antibody in plants exposed to long (D) or shorter (E) periods of limited light or threated with cycloheximide before returning to light (F). Total HYL1 accumulation, expressed relative to sample in lane 1 and measure as the sum of hypo- and hyper-phosphorylated HYL1 band intensities, is given in the uppermost line. Ratios between the hyper- and hypophosphorylated forms are given next. Cycloheximide addition is noted in (F) as CHX. The split blots in (F) show two fragments of the same autoradiography film produced from a single experiment.

(G) Phosphoprotein mobility shift gels probed with anti-HYL1 antibody. Ratios between the hyper- and hypophosphorylated HYL1 forms are given on top. Seedlings were transferred in dark or under green light to a medium containing 50 μM DCMU or mock solution 1 hr before transferring the plants to light.

(H) Phosphoprotein mobility shift gels, probed with anti-HYL1 antibody, of samples extracted from roots, whole seedling, or seedling aerial tissues of plants exposed to different light conditions. Ten-day-old seedlings grown LD, 10-day-old seedlings transfer for 2 days to dark (D), and then returned to white light for 2 hr (L).

(I) HYL1 (top) and HYL1-phosphoisoforms (bottom) accumulation in 10-day-old Col-0, *cpl1-7*, and *cpl1-7/cpl2-2* plants transferred to the dark or kept in an LD photoperiod (Light) for 4 days. The ratio of HYL1, or phosphorylated HYL1, between light and dark conditions is given on the top of each gel. Actin (ACT) or Coomassie staining were used as loading controls. On the right is noted the molecular weight.

(J) HYL1 accumulation in *hyl1-2* transformed with HYL1 phosphomimetic mutants. Plants were grown for 10 days and transferred to simulated shade or light. Relative band intensity is noted on top. S42A/D or S159A/D indicate individual mutations of serines 42 or 159 to alanine or aspartic acid respectively. On the right is noted the molecular weight.

In all panels, signal intensity was calculated using ImageJ.

undetectable after 2 days). Interestingly, a quick shift between HYL1 isoforms was observed, without large changes in total HYL1 levels, after seedlings were returned to white light (Figure 1D). Thus, a quick restoration of the active protein, at the expense of an inactive pool, was observed upon returning the plants to conditions providing adequate light supply. A more detailed analysis of the kinetics indicated that 1 day of darkness was sufficient to trigger active HYL1 degradation (Figure 1E) and that the recovery of the active HYL1 pool after returning to light was observed independently of the length of the dark incubation. Such change between HYL1 phosphoisoforms could be easily explained by a quick dephosphorylation of HYL1, but we could not exclude a rapid degradation of this form and the translation of fresh active isoform. To distinguish between these possibilities, we repeated the same kinetic but transferring the seedlings to liquid Murashige and Skoog medium containing 100 μM cycloheximide (CHX), a compound that inhibits translation, 2 hours before light restoration. After CHX treatment, only the non-phosphorylated HYL1 was detected, indicating that dephosphorylation of the inactive HYL1 reserve pool, rather than *de novo* translation, was the source of active HYL1 upon light restoration (Figure 1F). To test if a retrograde signal from the chloroplast is involved in the induction of HYL1 dephosphorylation upon transfer seedlings to light, we used 3-(3,4-dichlophenyl)1,1-dimethylurea (DCMU), a chemical compound that blocks the electron transfer from photosystem II to the plastoquinone pool, inhibiting any light-triggered signal coming from the chloroplast. Ten-day-old seedlings were transferred to darkness or simulated shade for 2 and 3 days, respectively, and then treated with or without 50 μM DCMU for 1 hr before returning the seedlings to white light. One hour after light restoration, samples were collected and HYL1 isoforms separated with Phos-tag gels. The results showed that the treatment with DCMU almost completely blocked the dephosphorylation of HYL1 triggered by light restoration (Figure 1G). This suggests that the signal leading to the reactivation of HYL1 is modulated by the chloroplast and potentially mediated by a mobile signal. In agreement with this idea, light-dependent degradation of HYL1, but most importantly the recovery of the active HYL1 pool after light restoration, took place but appeared to be partially impaired or delayed in roots compared with aerial tissues (Figure 1H). This may imply that a mobile signal from the leaves has to reach the roots to trigger the observed response. However, more evidence is necessary to confirm such a scenario. Despite it being more resistant to degradation than the active form, we observed a slow but consistent reduction of the phosphorylated HYL1 after long periods of light deprivation (Figures 1D and 1F). This could either mean that this isoform is also prone to degradation, at a slower rate, or that the equilibrium between isoforms is shifted upon the active HYL1 being degraded, leading to HYL1 dephosphorylation and further degradation. Additionally, we cannot exclude that the observed reduction in the active HYL1 form is the consequence of a dark- or shade-induced phosphorylation of this pool followed by the degradation of both isoforms. Since HYL1 is dephosphorylated mainly by CPL1 (Manavella et al., 2012), it would be expected, if our hypothesis is correct, that the phosphorylated form was more stable in *cpl1* mutant plants. We first evaluated HYL1 dark-induced degradation in *cpl1* mutant and found that the protein is more stable in such background, favoring our idea of phospho-protection of HYL1 (Figure 1I). Furthermore, when the phosphoisoforms were evaluated in the same plants, we found that in darkness the phosphorylated form became stabilized (Figure 1I). A partial degradation of HYL1 is still observed in *cpl1* mutants, as could be expected by the functional redundancy of this protein with CPL2 (Manavella et al., 2012). In agreement, the resistance to degradation is even more notorious in *cpl1/cpl2* double mutants (Figure 1I). This mutant, homozygous for the *cpl2-2* allele and heterozygous for the dominant negative *cpl1-7* allele (Manavella et al., 2012), confirmed the redundancy of both proteins controlling the phosphorylation of HYL1 and the resistance of this isoform to degradation. To further confirm that the phosphorylation of HYL1 renders it resistance to degradation, we made use of the previously described phospho-mimetic mutants of HYL1 (Manavella et al., 2012). *hyl1-2* mutants transformed with constructs mimicking phosphorylated serine 42 and serine 159 (S42D and S159D) and the corresponding dephosphorylated forms (S42A and S159A) (Manavella et al., 2012) were grown for 10 days and then transferred to simulated shade for 1 day. Such short incubation aimed to avoid full protein degradation, thus allowing us to visualize differences between the constructs. Western blot analysis showed that the phosphorylation of serine 159, but not serine 42, renders HYL1 insensible to degradation, supporting the stabilization of HYL1 upon phosphorylation during periods of limited light (Figure 1J). No significant differences between the expression levels of the different constructs were detected among the tested samples in control conditions (Figure S1I). Our result not only confirms the phospho-protection of HYL1 but also points to S159, and potentially the DRBM2 where it is located, as an important domain for such protection. However, we cannot exclude a role, even in protein stability, of other previously identified HYL1 phosphorylated amino acids (Manavella et al., 2012). Taken together, these results suggest that the inactive form of HYL1 forms a reserve pool of the protein during light starvation. In a given condition, such as after a proper light source is reached, this reserve pool is dephosphorylated to rapidly restore the active protein pool.

Distortion of the Balance between HYL1 Isoforms Impairs Growth Responses to Light, Shade, or Dark Conditions

The accumulation of the inactive HYL1 phosphorylated pool in darkness and its rapid dephosphorylation to restore protein activity upon light exposure suggests that HYL1 isoform dynamics could be important for the control of plant growth during de-etiolation. To address this issue, we used the HYL1 S>A phosphomimics (where both S42 and S159 were replaced by alanine; Manavella et al., (2012)), which cannot be phosphorylated and therefore lacks the protein reserve pool after prolonged darkness (Figure 1J). We followed a typical de-etiolation response, the unfolding of cotyledons in etiolated seedlings transferred from full darkness to white light. The lines expressing the HYL1 S>A and S159A phosphomimics opened the cotyledons at a slower rate, both when measured as the number of seedlings with open cotyledons (cotyledon opening >10°) and as the opening angle over time (Figures 2A, 2B, S2A, and S2B). The S42A mutants, where phosphorylation of S159 and the formation of the reserve pool are possible, behaved similar to control plants

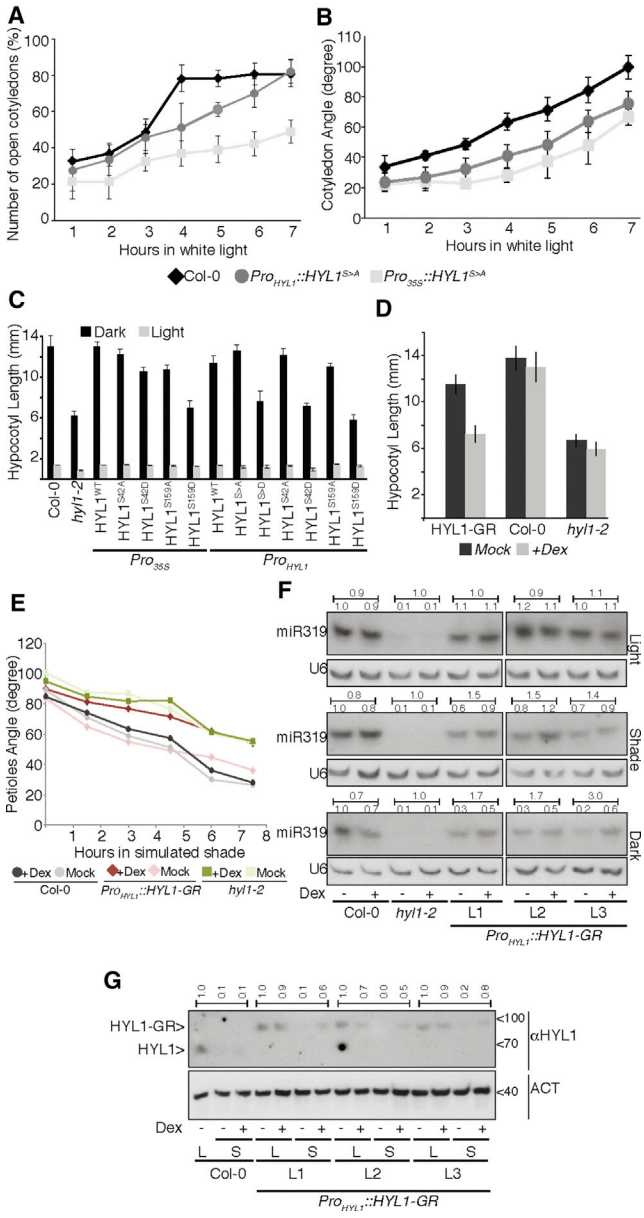

Figure 2. HYL1 Phosphorylation Balance Influences the Photomorphogenesis Response

(A) Number of plants with open cotyledons (>10° opening angel) at a given time.

(B) Opening angle of opened cotyledons.

(C and D) Hypocotyl length of 4-day-old seedlings germinated in dark or light (C) or in dark with (+Dex) or without (Mock) the dexamethasone (D). S > D/A indicates mutation of seven serine codons in HYL1 to alanine or aspartic acid respectively (Manavella et al., 2012). S42A/D or S159A/D indicates individual mutations of serines 42 or 159. HYL1 phosphomimics were cloned under the cauliflower mosaic virus 35S promoter (Pro_{35S}) or the HYL1 regulatory region (Pro_{HYL1}). HYL1 fused to the glucocorticoid receptor (HYL1-GR).

(E and F) (E) Closing angle of petioles, from leaves 1 and 2, over time after transferring 15-day-old seedlings a from LD photoperiod to simulated shade. (F) RNA blots for detection of miR319 in LD-grown plants transfer to light, shade, or darkness and treated with dexamethasone or mock solution. U6 hybridization was used as loading control. In the uppermost line of each blot the intensity ratio between the treated versus untreated sample is shown. Three independent transgenic lines (L1–L3) are shown.

(Figures S2A and S2B). These results suggest that a quick restoration of active HYL1 is required for a proper developmental response during the dark-to-light response.

We next investigated if the selective degradation of the active non-phosphorylated HYL1 during prolonged periods of dark or shade is also physiologically relevant. To test this idea, we germinated *hyl1-2* mutant plants complemented with different variants of the *HYL1* gene in complete darkness and measured the hypocotyl length. The hypocotyl elongates substantially in darkness, pushing the cotyledons out of the soil to rapidly initiate photosynthesis, and is a good parameter to evaluate dark response. Expression of the wild-type (WT) *HYL1*, or the non-phosphorylated mimics, that are degradation sensitive, under the control of either the *35S* or the *HYL1* promoters, successfully complemented the *hyl1-2* phenotype and showed normal hypocotyl elongation (Figure 2C). In contrast, the lines expressing the phosphorylated HYL1 mimic S159D, which is particularly resistant to degradation (Figure 1J), showed shorter hypocotyls (Figure 2C), suggesting that HYL1 degradation is required for proper skotomorphogenesis. The S42D and S159D HYL1 phosphorylated mimics, which are inactive (Manavella et al., 2012), also failed to complement *hyl1-2* phenotype (Figure 2C and Lu and Fedoroff (2000)). Therefore, normal hypocotyl growth in darkness requires accumulation of a minimal level of the normal protein. While the above experiments are consistent with a role of HYL1 degradation in darkness, they could also be interpreted in terms of the requirement of a minimum activity of HYL1 in darkness, and the phosphorylated HYL1 mimic S159D is unable to provide this activity. Therefore, we followed an additional approach aiming to bypass the cytoplasmic HYL1 degradation without affecting the protein activity, in order to conserve an active pool of the protein in darkness. With this objective, we fused the *HYL1* coding sequence to the glucocorticoid receptor (GR), cloned the cassette under the control of the *HYL1* promoter, and used it to transform *hyl1-2* mutant plants. Like many other steroid receptors, the GR will remain in the cytoplasm until a ligand is bound and triggers its translocation to the nucleus, where it fulfills its functions (Brockmann et al., 2001). Thus, GR keeps the fused HYL1 largely in the cytoplasm, where it can be actively degraded during the dark or shade. Upon treatment of plants with dexamethasone (DEX), the fusion protein will move to the nucleus, confining HYL1-GR to this compartment during dark or shade, and avoiding its degradation. Transgenic seeds were germinated in the dark in growth medium with or without DEX, and once more the plant response to light deprivation was measured as hypocotyl length. HYL1-GR plants treated with the steroid analogue presented shorter hypocotyls than mock-treated plants (Figure 2D), reinforcing the idea that an active degradation of non-phosphorylated HYL1 is required for normal skotomorphogenesis. Leaf hyponasty (the elevation of the leaves, closing the angle between them, due to enhanced growth of the abaxial layers of cells) is a typical response of

(G) Western blot quantification of HYL1 in plants treated as in (F). Plants transferred to light (L) or shade (S) are displayed. Signal intensity, calculated with ImageJ, is shown relative to each line: light grown, mock treated, control. On the right is noted the molecular weight.

In all cases, error bars show 2× SEM. p values of less than 0.05 in a t test with Bonferroni's correction were considered significant.

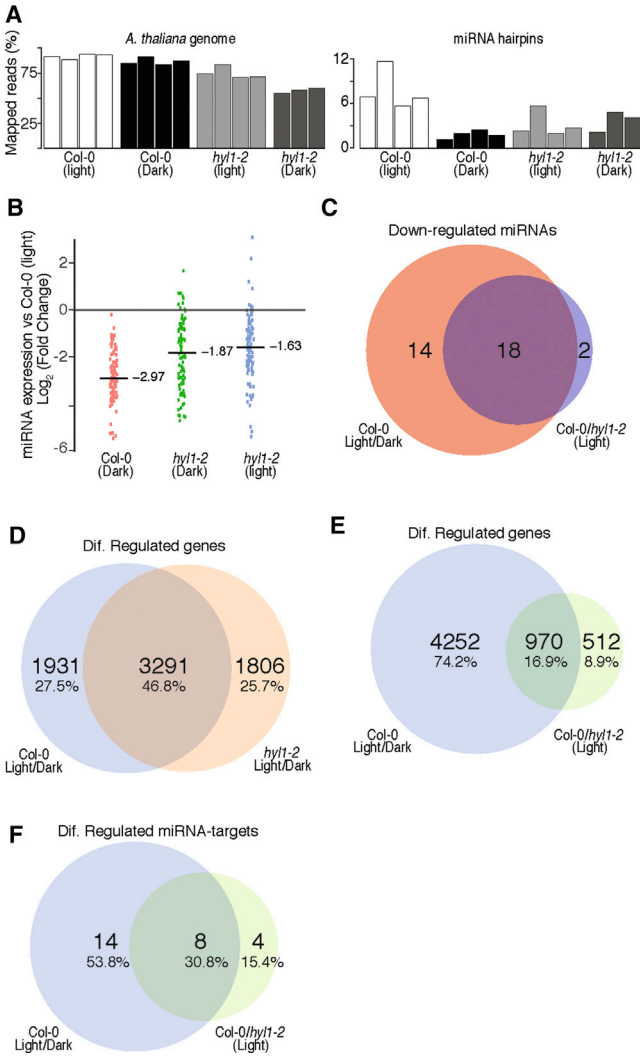

Figure 3. HYL1 Degradation/Reactivation Impacts miRNA Production and Targets Silencing

(A) Percentage of small RNA sequencing (RNA-seq) reads mapped to the *Arabidopsis* genome (left) and to miRNA hairpins (right). Each bar represents a biological replicate.

(B) Mean expression levels of individual miRNAs in dark-grown Col-0 plants and in light- or dark-grown *hyl1-2* plants with respect to light-grown Col-0 plants. Horizontal segments indicate the median of the expression levels. Each dot corresponds to a single miRNA or collapsed miRNA family.

(C) Venn diagram presenting the overlap of miRNAs downregulated in dark- versus light-grown Col-0 plants against those regulated in Col-0 versus *hyl1-2* plants grown in light conditions.

(D and E) Venn diagrams comparing (D) light- or (E) genotype-dependent differentially expressed genes in Col-0 and *hyl1-2* mutants.

(F) Venn diagrams comparing differentially expressed miRNA targets in different backgrounds and light conditions.

plants exposed to neighbor shading. We measured the angle between the leaves in plants exposed to prolonged shade. The DEX-treated HYL1-GR transgenic plants presented a delayed leaf hyponasty compared with the mock-treated plants (Figure 2E). The expectation of high HYL1 activity in HYL1-GR plants treated with DEX is met by the results showing higher miR319 levels under this condition than in the mock-treated 10-day-old plants transferred to shade or darkness (Figure 2F). MiR168 levels, normally unaffected in *hyl1* mutants, did not show any fluctuation between the tested conditions (Figure S2C). Additionally, quantification of HYL1 levels in the same samples confirmed the efficiency of DEX treatment to protect, at least partially, HYL1 from degradation (Figure 2G).

Light-Quality-Mediated Regulation of HYL1 Impacts the miRNA Production, Affecting the Expression of Developmentally Important Genes

Our results show that a harmonious balance between HYL1 degradation and reactivation, mediated by changes in HYL1 phosphorylation, is necessary for plant responses to prolonged darkness or shade and to the transition between these conditions and light. Therefore, we decided to investigate the molecular signature associated with the growth phenotypes. Since HYL1 is a core miRNA biogenesis factor, and a large number of miRNA targets control plant development, we analyzed miRNA and miRNA-target populations by small RNA and mRNA sequencing during dark-to-light transition. In order to analyze such profiles, Col-0 WT and *hyl1-2* mutant plants were grown for 10 days under long-day photoperiod (16 hr light/8 hr dark), and then either transferred to darkness (simulated reburial) or left under the long-day cycles for 72 hr. Small RNA sequencing revealed a drastic reduction in miRNA accumulation in response to darkness, while the general population of other small RNAs mapping the *Arabidopsis* genome were not affected (Figures 3A and 3B). Notoriously, the general reduction in miRNAs is comparable with the impact of the *hyl1-2* mutation. Among 145 miRNA families tested, we collapsed miRNA family members with identical sequence, 105 were above our expression threshold in the tested samples. We detected a significant reduction in 34 miRNAs, which represents 32.4% of the expressed miRNA families. Most importantly, when we compared the differentially expressed miRNA families between Col-0 light/Col-0 dark and Col-0 light/*hyl1-2* light, there was a remarkable overlap of downregulated miRNAs (Figure 3C). We analyzed our RNA sequencing data to evaluate if the observed reduction in miRNA population was the consequence of a dark-induced repression of their encoding genes. Among all pri-miRNA transcripts above a detection threshold, a few, such as pri-miR159b, pri-miR163, and pri-miR157c, were induced in dark, while we only detected pri-miR172 as repressed in dark. These results indicate that the miRNA population of dark-adapted plants resembles the miRNA population of the *hyl1-2* mutant, which is consistent with the observed HYL1 degradation in darkness. As reported for *hyl1-2* mutants, not all miRNAs are significantly reduced in dark-adapted plants (Table S1). Repressed miRNAs families include miR159a, b (which regulates MYB transcription factors), miR319a-c (which regulates TCP transcription factors), miR390a,b (which regulates TAS3>ARF), and miR396a (which regulates GRF), all of them known to be important for plant development and even hypocotyl elongation. We performed small RNA blots to confirm that these developmentally important miRNAs are repressed upon a plant being transferred to dark and quickly recover after light restoration (Figure S3A).

As expected, the light versus dark conditions had per se large effects on the transcriptome, independently of the

HYL1-asociated miRNA pool. Over 46% of the dark-regulated genes in Col-0 are also regulated by dark in *hyl1-2* mutant (Figure 3D). However, a comparison of the dark-regulated genes in Col-0 with the HYL1-regulated transcript also showed a significant overlap of the regulated genes, 16.9%, which is more than expected by chance (Fisher test p value = 2.2^{-16}, Figure 3E). These results are consistent with the requirement of miRNA depletion during prolonged darkness to shape the response at transcriptional level. When we repeated the same analysis but only focusing on known miRNA targets, the overlap became even more evident, reaching 30.8% of the regulated genes (chi squared test p value < 0.1, Figure 3F). Among the regulated genes, those encoding developmentally important transcription factors (such as TCP4, 2, and 10; ARF8 and 16; GRF2, 4 and 7 and MYB33) appeared (Table S2). RT-qPCR analysis confirmed that these transcription factors were indeed upregulated during dark periods, presumably by a miRNA-silencing release, and repressed again after light restoration (Figure S3B). Upon light restoration, the dephosphorylation of the HYL1 reserve pool re-activates miRNA production, restoring gene silencing to allow the switch between developmental programs during the dark/light transition.

An Exclusive Nuclear Localization of Monomeric Phosphorylated HYL1 Protects It from Degradation

The above results show that a degradation-resistant pool of phosphorylated HYL1 is essential, under prolonged darkness or shade, to quickly restore miRNA biogenesis and mediate physiological responses when the plants are re-exposed to a proper light source. However, it is unclear how the phosphorylation of HYL1 renders it capable of escaping cytoplasmic degradation. In order to test if the phosphorylation of HYL1 affects its nuclear/cytoplasmic partition, and therefore its degradation, we fused the WT and phosphomimic versions of HYL1 to the GFP, cloned the tagged constructs under the *HYL1* regulatory region, and transformed *hyl1-2* mutants. We also cloned the constructs under the *35S* promoter to force the over-accumulation of the protein. Using these lines, we analyzed HYL1 localization in plants kept either in light or darkness for 24 hr. As previously reported, the overexpressed WT version of HYL1 in *Arabidopsis* was located in both the nucleus and the cytoplasm (Cho et al., 2014; Zhang et al., 2017) (Figure 4A). In the tested conditions, ectopic overexpression of the tagged protein was sufficient to compensate for HYL1 degradation in darkness, allowing us to detect the protein in both compartments even in the dark (Figure 4A). This was not the case for the HYL1 promoter lines where, as reported, the cytoplasmic portion was degraded in the dark (Figure 4A). All the constructs where serines were mutated to alanine, mimicking a non-phosphorylated HYL1, shared the same cellular localization pattern as the WT version (Figure 4A). However, and despite the usage of the *35S* promoter, the HYL1 fully phosphorylated mimic (S>D) and the S159D, but not the S42D, were largely restricted to the nucleus of the cell, both in light and darkness (Figure 4A). Fusion protein levels, as well as fluorescence intensity in the nuclei, were quantified to exclude variation in the expression levels and to confirm the stability of the nuclear protein (Figures S4A and S4B). These results imply that the phosphorylation of HYL1 S159 restricts its subcellular localization to the nucleus, where it will avoid cytoplasmic degradation. To test this hypothesis, we isolated proteins from nuclear and cytoplasmic cellular fractions and used Phos-tag gels to quantify HYL1 isoforms. The results revealed an enrichment of phosphorylated HYL1 in the nucleus and a depletion in the cytoplasm (Figure 4B). As expected, the active non-phosphorylated HYL1 isoform is present both in the nucleus, where it fulfills its function in miRNA processing, and in the cytoplasm, where it is actively degraded during light deprivation. Based on this experiment, the following HYL1 pools can be defined: the dephosphorylated pool, the active nuclear pool, the phosphorylated inactive nuclear pool, and the dephosphorylated cytoplasmic pool.

Thus, the observed degradation resistance of phosphorylated HYL1 could be the result of its preferential nuclear localization, which in turn protects it from an undefined cytoplasmic protease. The exclusive nuclear localization of the S159D mutant, but not S42D, is in agreement with the observation that only the phosphorylation of this residue protected HYL1 from degradation (Figure 1J). Conversely, when we forced the S159D phosphomimic to stay in the cytoplasm, by fusing it to the GR receptor, it was degraded almost as efficiently as the non-phosphorylated form (Figure 4C). This observation reinforces the idea of the nuclear protection of the phosphorylated HYL1, and implies that the phosphorylation itself is not responsible for the protein stability but for controlling its subcellular localization.

Aiming to understand how phosphorylation affects HYL1 activity and stability, we performed HYL1-pri-miRNA co-immunoprecipitation experiments and protein-protein interaction assays. Using a HYL1-specific antibody, we immuno-precipitated the different phosphomimics expressed in the *hyl1-2* mutant background. Associated RNAs were then purified and used for cDNA synthesis followed by PCR to detect the interacting pri-miRNAs. All phosphomimics analyzed, with the exception of S42D, were able to interact with the tested pri-miRNAs (Figure 4D). Considering the role of the DRBM1, where S42 is located, in HYL1-pri-miRNA interaction (Yang et al., 2010), the failure of S42D to properly interact with the pri-miRNAs could be expected and might explain its impaired activity. However, the pri-miRNA-binding capacity of S159D suggested that the HYL1 RNA binding capacity does not influence its stability or preferential nuclear localization. We also evaluated the capacity of HYL1 and the phosphomimics to interact with its known partner SE and to form dimers (Yang et al., 2014). Interestingly, yeast two-hybrid assays (Y2H) revealed that the phosphorylation of S159 impairs both its capacity to interact with SE and to form homodimers (Figures 4E and S4C). In agreement with our Y2H results, it was reported that two β sheets of the DRBM2, where S159 is located, are necessary for HYL1 dimer formation (Yang et al., 2010). The fact that HYL1 S159D is mainly located in the nucleus and fails to interact with SE, or dimerize, suggests a potential dependency of HYL1 to associate with chaperon proteins for its movement to the cytoplasm, as is the case of the HYL1 nuclear import (Zhang et al., 2017). If this hypothesis is correct, we would observe a differential distribution of HYL1 monomers and dimers in the nucleus and cytoplasm. To further investigate the subcellular distributions of HYL1-containing complexes, we combined cell fractioning and gel filtration assays. The purity of nuclear/cytoplasmic fractioning was confirmed by measuring subcellular marker proteins (Figure S5A). In the nucleus, HYL1

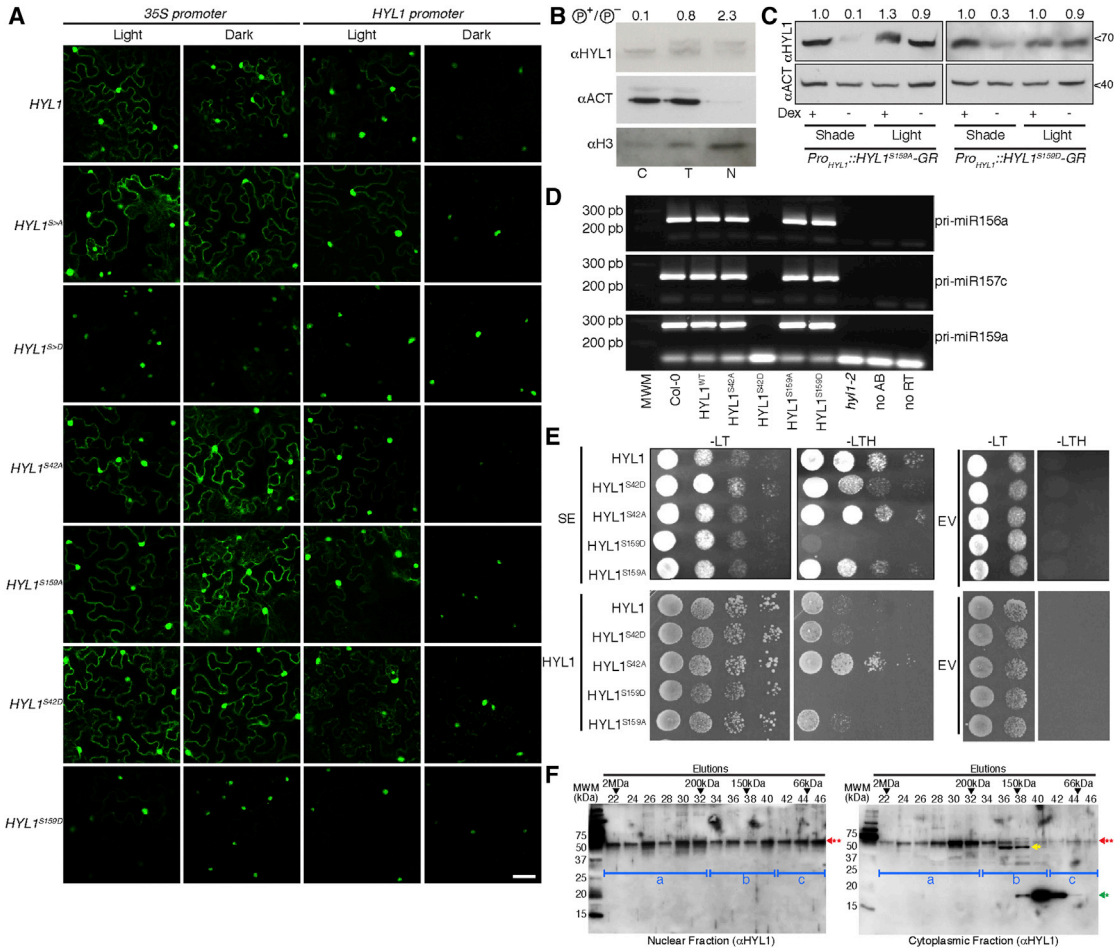

Figure 4. The Nuclear Localization of the Phosphorylated HYL1 Protects It from Degradation

(A and B) (A) Nuclear/cytoplasmic localization of eGFP-tagged HYL1 and HYL1 phosphomimics, expressed under the cauliflower mosaic virus 35S promoter or the endogenous *HYL1* regulatory sequence. S > D or S > A indicates mutation of seven serine codons in HYL1. S42A/D or S159A/D indicates individual mutations of serines 42 or 159 (Manavella et al., 2012). Plants were kept in light or 24 hr in dark before image acquisition. All images are recorded with the same magnification. Scale bar on the bottom right panel represent 50 μm. (B) Phosphoprotein mobility shift gels probed with anti-HYL1 antibody of samples extracted from subcellular fractionations (cytoplasm [C] and nucleus [N]) or total protein extract (T). Ratios between the phosphorylated and non-phosphorylated HYL1 forms are given at the top of each band pair. Detection of ACTINE (ACT) and HISTONE3 (H3) in each sample was used as control of fraction purity (ACT cytoplasmic and H3 nuclear).

(C) Western blot quantification of HYL1-GR fusion protein in plants treated with dexamethasone (Dex+) or mock solution (−) and transfer to simulated shade or kept in long-day photoperiod for 2 days. Relative signal intensity, calculated with ImageJ, is shown on top.

(D) RNA immunoprecipitation assay performed using an anti-HYL1 antibody. HYL1 phosphomimics-associated pri-miRNAs were detected by RT-PCR. *hyl1-2* mutant plants were used as a negative control for unspecific binding. "no AB" shows RT-PCR performed on samples to which no antibody was added during the RNA immunoprecipitation protocol. "no RT" shows PCR performed directly on the RNA immunoprecipitation as a control of genomic DNA contamination.

(E) Yeast two-hybrid assay. SERRATE (SE) and HYL1 were fused to the GAL4 binding domain; HYL1 mutants to the GAL4 DNA activation domain; a vector (EV) only expressing the GAL4 binding domain was used as control. -LT, medium without leucine and tryptophan; -LTH, without leucine, tryptophan, and histidine. Serial 1:10 dilutions are shown. Full series of dilution in the EV controls are shown in Figure S4C.

(F) Size-exclusion chromatography of HYL1 in the nuclear (left) and cytoplasmic (right) fractions. HYL1 supercomplexes, dimeric HYL1, and monomeric HYL1 are noted as a, b, and c respectively. Two red asterisks indicate full-length HYL1. Single green asterisk indicates cleaved N-terminal products of HYL1. Single yellow asterisk indicates cleaved C-terminal products of HYL1.

was detected as high-order protein complexes (over 200 kDa), which may represent HYL1 associated with the miRNA processing complex, association with its multiple known interactors (Achkar et al., 2016) or forms of self-assembled multi-complex such as tetramer, as previously shown (Yang et al., 2010) (Figure 4F). A strong signal was also detected in the fractions that represent HYL1 dimers (~150 kDa) and monomers (~66 kDa). In the cytoplasm, HYL1 was mostly found as higher-order protein complexes (~200 kDa) (Figure 4F). Cytoplasmic dimers and monomers were barely detected and may represent only recently translated protein. The phosphorylated HYL1, which was preferentially detected in the nucleus and failed to form dimers, may comprise the nuclear monomeric protein detected in these experiments. However, further experiments are

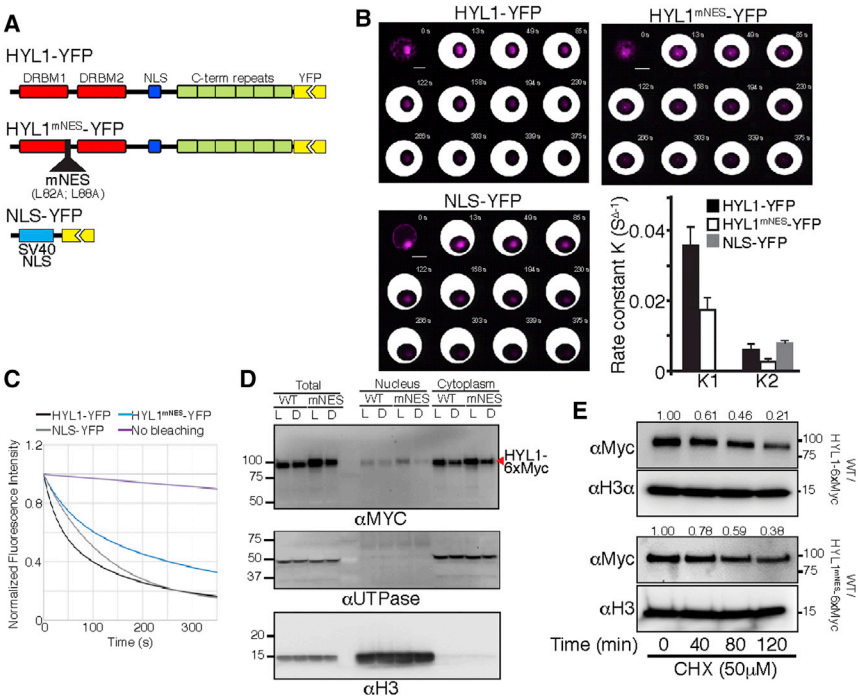

Figure 5. HYL1 Changes Subcellular Localization in Response to Light and Dark Transitions

(A) Graphical representation of the HYL1-YFP, HYL1^{mNES}-YFP, and NLS-YFP constructs.

(B) FLIP analysis of HYL1-YFP, HYL1^{mNES}-YFP, and NLS-YFP in *Arabidopsis* protoplasts. A large cytoplasmic area enclosing the nucleus was continuously photobleached and the average intensity in the nucleus was measured over time. The montage shows loss of fluorescence in the nucleus over time. Scale bars represent 10 μm. Fluorescence intensity of the nucleus was background subtracted and decay curves from each nucleus were fitted using GraphPad to obtain the rate constants K1 and K2 (s^{-1}). NLS-YFP showed a single exponential decay curve. Error bars show 2× SEM. p values of less than 0.05 in a t test with Bonferroni's correction were considered significant.

(C) Normalized recovery curves calculated from plateau, K1 and K2.

(D) Protein stability of HYL1-6xMyc and HYL1^{mNES}-6xMyc in response to dark as detected with α-Myc antibody. Fidelity of subcellular fractionation was confirmed with α-UTPase and α-histone antibodies. Samples were collected from plants transferred to light (L) or dark (D) for 12 hr.

(E) Degradation rate of HYL1-6xMyc and HYL1^{mNES}-6xMyc. Ten-day-old transgenic seedlings were incubated in liquid MS medium with 50 μM cycloheximide (CHX) for 15 min and sampled at the indicated time points and determined with α-Myc antibody.

necessary to confirm the identity of this nuclear pool. Additionally, the small amount of dimeric and monomeric HYL1 in the cytoplasm may indicate either that these fractions were preferentially degraded in the cytoplasm or that protein dimerization is necessary for nuclear export (Figure 4F, left panel). Potential protease-cleaved fragments of HYL1, N-terminal fragment (green arrow), and C-terminal fragment (yellow arrow) were detected only in the cytoplasm and in the exclusion fraction corresponding to the predicted size of a dimer (~150 kDa) (Figure 4F). This observation suggests that HYL1 degradation might take place from dimeric HYL1 substrates. Nevertheless, the dark-induced degradation of HYL1 S159D phosphomimic when forced to be located in the cytoplasm (Figure 4C) suggested that monomers could also be degraded as efficiently as dimers. Thus the apparent specific degradation of dimeric HYL1 in the experiment shown in Figure 4F may reflect the preferential dimeric state of the protein in the cytoplasm. However, additional experimentation, especially after the identification of HYL-dedicated protease, will be necessary to understand the mechanisms involved in HYL1 cytoplasmic degradation.

HYL1 Behaves as a Nuclear-Cytoplasmic Shuttling Protein in Response to Light and Dark Transition

HYL1 is a well-known nuclear protein and a recent study reported that KETCH1 imports HYL1 into the nucleus (Zhang et al., 2017). Consistently, we were able to record the active translocation of HYL1-YFP into the nucleus using fluorescence recovery after photobleaching (FRAP) assay (Figure S5B). Two components, K1 (fast) and K2 (slow) recovery rate constants, were obtained (Figures S5C and S5D). K1 corresponds to the active shuttling of HYL1-YFP into the nucleus, potentially mediated by KETCH1, while K2 corresponds to the passive diffusion of HYL1-YFP (Figures S5B–S5D). Considering that the proteolysis of HYL1 occurs only in the cytoplasm (Cho et al., 2014), the dark-induced degradation of non-phosphorylated HYL1 could be explained if HYL1 is a nuclear-cytoplasmic shuttling protein. A bioinformatic analysis of HYL1 protein sequence revealed the presence of a putative nuclear export signal (NES) between amino acids 79 and 92 (LRE**L**AKSSE**L**SQCV) (Figure 5A). In order to investigate whether this NES facilitates the cytoplasmic export of HYL1, we created a HYL1 version (HYL1^{mNES}-YFP) containing two amino acid substitutions (L82A, L88A) in the NES sequence (Figures 5A and S5E). Using fluorescence loss in photobleaching (FLIP) assay, we investigated the cytoplasmic shuttling of HYL1-YFP, HYL1^{mNES}-YFP, and NLS-YFP as a control. In darkness, a large proportion of the cytoplasm was continuously bleached and the fluorescence intensity of HYL1 in the nucleus was measured (Figure 5B). Two-component decay fits (K1 and K2) were recorded for HYL1-YFP and HYL1^{mNES}-YFP, whereas NLS-YFP only showed a single-component decay (K2) (Figure 5B). The K1 constant of HYL1 showed a fast and active nuclear export. The rate of nuclear export of HYL1^{mNES}-YFP was significantly slower ($p < 0.05$), implying that the mutations in the NES notably hindered HYL1 export to the cytoplasm under dark condition (Figure 5C). The K2 constant was not significantly altered among tested proteins. The similarity between K2 values of HYL1-YFP and NLS-YFP indicated that a preferentially nuclear retained fraction of HYL1, potentially the phosphorylated version, coexist with a shuttling component (Figure 5B). The exporting kinetics showed that the nuclear export of HYL1-YFP

reaches a plateau within 350 s, while HYL1^{mNES}-YFP would eventually reach it after 1,500 s (Figure 5C). This suggested that, even when important for the nuclear export, the NES is not the only component directing such process. In line with this result, a nuclear/cytoplasmic fractioning of plants kept for 12 hr in light or darkness showed that the HYL1^{mNES}-YFP mutant is still exported to the cytoplasm and finally degraded (Figures 5D and S5F). The degradation of the HYL1^{mNES}-YFP mutant in this experiment would argue against our results showing the nuclear protection of the phosphorylated protein. However, the NES mutations only slow down the export of HYL1 to the cytoplasm but do not to block it completely (Figure 5C). Thus, it could be expected that this mutant is also eventually degraded after a long dark incubation such as the one used in this experiment. To solve this discrepancy, we performed a CHASE-ASSAY experiment that allowed us to score more precisely the stability of this mutant protein in a short time lapse. The experiment showed that, despite being degraded at a certain point, the HYL1^{mNES} degradation rate is slower than the WT protein (Figure 5E). This result is compatible with the nuclear protection of HYL1 and the slower nuclear-cytoplasmic export of HYL1^{mNES}. In this sense, a HYL1^{mNES}-6xMyc construct was able to complement *hyl1-2* morphological phenotype and miRNA production but presented slightly shorter hypocotyls than WT plants when grown in dark (Figures S5G–S5J). These results were consistent with the HYL1-GR analysis and reinforced the hypothesis that an efficient cytoplasmic degradation of the active HYL1 is necessary for a proper light response.

DISCUSSION

HYL1 is a central component of the plant miRNA biogenesis machinery that can be present in a dephosphorylated (active) or phosphorylated (inactive) form (Achkar et al., 2016). However, the biological relevance of this post-translational regulation has remained elusive. Here we show that the phosphorylation of HYL1 generates a reserve pool of inactive protein resistant to dark- or shade-induced proteolytic degradation (Figure 1). After a prolonged period of dark or shade, and when the plants return to more favorable conditions of light availability, a quick dephosphorylation of the reserve pool restores HYL1 activity and miRNA biogenesis (Figure 1). These shifts in HYL1 are important for the developmental transitions that take place during prolonged darkness or shade and upon the subsequent exposure to light (Figure 2).

Mechanistically, the phosphorylation of HYL1 at serine 159 protects the protein from degradation by restricting its localization to the nucleus (Figure 4A). The phosphorylation of this serine, located in the DRBM2 domain, also impairs HYL1 dimerization and interaction with SE (Figure 4E). These observations suggest that the exclusive nuclear localization of phosphorylated HYL1, and therefore its stability, may respond to its failure to interact with partner proteins. This would imply that the nuclear export of HYL1 is mediated by the interaction with DRBM2-associated proteins. Nevertheless, it is also possible that the phosphorylation at DRBM2 produces a conformational change that hides the closely located NES, partially blocking its nuclear/cytoplasmic transport. Our results are in agreement with the reports in animal systems showing that the functional homologs of HYL1 (TRBP and DGCR8) are stabilized by phosphorylation (Herbert et al., 2013; Paroo et al., 2009). The proposed nuclear stability of phosphorylated HYL1 is also supported by the observation that, in the absence of SnRK2 kinases, required for nuclear phosphorylation of HYL1, the protein becomes destabilized during osmotic stresses (Yan et al., 2017). However, these observations are at odds with a recent report claiming that HYL1 phosphorylation leads to the protein de-stabilization and degradation and that dephosphorylation, by Protein Phosphatase 4 (PP4)/SMEK1 complex, stabilizes HYL1 (Su et al., 2017). A likely explanation of this discrepancy could be based on the use of a cell-free protein decay assay to test HYL1 stability where cells are disrupted and the nuclear-cytoplasmic partitioning, which we found to be crucial for the control of stability (Figure 3), is lost. This is in line with our observation that the phosphorylation of HYL1 per se is not responsible for the stability of this form but rather its exclusive nuclear localization (Figure 4C). Furthermore, even when recombinant HYL1 is degraded in a cell-free assay, it is not phosphorylated in such conditions (Figures S5K and S5L). Our proposal that phosphorylation stabilizes HYL1 *in vivo* while the dephosphorylated form is degraded is also consistent with Phos-tag gels shown by Su et al. (2017), where only the non-phosphorylated form is reduced in *smek* mutants, while the phosphorylated form is largely unaffected.

Several pieces of evidence support a significant role of the dynamic patterns of light-controlled HYL1 phosphorylation on the adjustment of plant developmental patterns, and their associated gene expression signatures, to the prevailing environmental light conditions. For example, we found that distortion of the HYL1 phosphorylation kinetics reduced hypocotyl growth in young seedlings exposed to simulated burial (full darkness) and reduced the hyponastic leaf growth in plants exposed to prolonged simulated shade from neighbors. These mutant growth patterns are predicted to impair the chances of the foliage to reach light emerging either from the soil or from the shading canopy, respectively. At molecular level, simulated re-burial (transfer of light-grown plants to full darkness) repressed a group of developmentally important miRNAs, including miR159, miR319, miR390, and miR396, giving rise to a concomitant increase in the expression of their targets. These targets include MYB, TCP, ARF, and GRF transcription factors, which are likely to mediate the growth responses observed (Alonso-Peral et al., 2010; Rodriguez et al., 2010; Sarvepalli and Nath, 2011).

While the response to prolonged darkness or shade is inevitably slow because it involves measuring the duration of the signal, the response to subsequent light has to be rapid to maximize its benefits. We observed a rapid accumulation of the active pool of HYL1 at the expense of the inactive reserve pool, mediated by a quick dephosphorylation of HYL1, upon light becoming available after a prolonged period of dark or shade (Figure 1). This quick phosphorylation shift was required for the normal unfolding of the cotyledons (Figure 2), a growth response that rapidly exposes the photosynthetic tissues to light during de-etiolation.

While the inactive form of HYL1 is the most abundant in mature organs such as leaves, developed flowers, roots, and siliques, the active form dominates in young seedlings and young organs. This unequal distribution may reflect a greater need for

miRNA-mediated gene regulation in early stages of development. Strong degradation of the active form of HYL1 occurred in light-grown plants transferred to simulated reburial conditions (full darkness) or simulated shade (low light levels, proportionally enriched in far-red light). Conversely, HYL1 was only slightly affected by the duration of darkness during the day/night cycle and this had no detectable consequences on the miRNA levels, suggesting that brief periods of reduced HYL1 do not affect miRNA production. Thus, the degradation of active HYL1, and the formation of an inactive reserve pool able to affect miRNA production, occur in response to unusually prolonged periods of limiting photosynthetic input. The pathways involved between the light versus darkness or shade cues and the phosphorylation of HYL1 are not clear but, in light-grown plants, inhibitors of photosynthesis impair the light response, suggesting a role of retrograde signals from the active chloroplasts.

The abundance of HYL1 in the cytoplasm may also imply a function of this protein in this cellular compartment, as is the case for some of the HYL1 homologs (Eamens et al., 2012). The identification of HYL1 proteases will be an important milestone to understand the cell-signaling cascade regulating HYL1 activity and therefore miRNA biogenesis.

Plant plasticity to bear the challenges imposed by fluctuations in light availability depends on the ability to integrate environmental cues at different time scales and combine rapid and reversible responses with longer-term modifications (Casal et al., 2004). Here we show that slow kinetics of HYL1 de-activation (degradation plus phosphorylation) and the rapid re-accumulation of HYL1 by de-phosphorylation of the inactive reserve pool provide a molecular mechanism to combine gradual acclimation under periods of prolonged light scarcity with rapid re-adjustment when more favorable light conditions are restored.

STAR★METHODS

Detailed methods are provided in the online version of this paper and include the following:

- KEY RESOURCES TABLE
- CONTACT FOR REAGENT AND RESOURCE SHARING
- EXPERIMENTAL MODEL AND SUBJECT DETAILS
  - Plant Material
- METHOD DETAILS
  - Light Conditions
  - Temperature and Pharmacological Treatments
  - Plasmid Construction
  - Plant Transient Transformation
  - RNA Analysis
  - RNA and Small RNA Sequencing
  - Microscopy
  - FRAP and FLIP Analyses
  - Cycloheximide (CHX)-Chase Assay
  - Cell Fractionation and Size-Exclusion Chromatography Analyses
  - Protein Analyses
  - Cell-Free HYL1 Degradation and Phosphorylation Assay
  - RNA Immunoprecipitation Assay
- QUANTIFICATION AND STATISTICAL ANALYSIS
- DATA AND SOFTWARE AVAILABILITY

SUPPLEMENTAL INFORMATION

Supplemental Information includes five figures and four tables and can be found with this article online at https://doi.org/10.1016/j.devcel.2018.06.014.

ACKNOWLEDGMENTS

This work was supported by grants from ANPCyT (Agencia Nacional de Promoción Científica y Tecnológica, Argentina), HFSP (Human Frontier Science Program), and the Max Planck Society, ICGEB (International Centre for Genetic Engineering and Biotechnology) to P.A.M.; Basic Science Research Program through the National Research Foundation of Korea (NRF) funded by the Ministry of Science, ICT and Future Planning (grant number: NRF-2017R1A2B4010255), the VILLUM Research Center "Plant Plasticity", and the Center for Synthetic Biology "bioSYNergy" (UCPH Excellence Programme for Interdisciplinary Research) to S.W.Y.; NRF-2016R1C1B1013506 to S.K.C.; and NRF-2017R1A6A3A11035981 to M.Y.R. P.A.M., J.J.C., A.L.A., and D.A.R. are members of CONICET; N.P.A. is a fellow of the same institution.

AUTHOR CONTRIBUTIONS

Conceptualization and Methodology, N.P.A., S.K.C., C.P., S.W.Y., and P.A.M.; Investigation, N.P.A., E.K., A.J.G., J.J.C., S.K.C., C.P., S.W.C., and M.Y.R.; Formal Analysis, A.L.A. and D.A.R.; Supervision, P.A.M., S.W.Y., J.J.C., and J.H.; Writing – Original Draft, N.P.A., J.J.C., S.W.Y., and P.A.M.; Writing – Review & Editing, all authors.

DECLARATION OF INTERESTS

The authors declare no competing interests.

Received: July 11, 2017
Revised: March 14, 2018
Accepted: June 19, 2018
Published: July 16, 2018

REFERENCES

Achkar, N.P., Cambiagno, D.A., and Manavella, P.A. (2016). miRNA biogenesis: a dynamic pathway. Trends Plant Sci. *21*, 1034–1044.

Alonso-Peral, M.M., Li, J., Li, Y., Allen, R.S., Schnippenkoetter, W., Ohms, S., White, R.G., and Millar, A.A. (2010). The microRNA159-regulated GAMYB-like genes inhibit growth and promote programmed cell death in *Arabidopsis*. Plant Physiol. *154*, 757–771.

Ballare, C.L., and Pierik, R. (2017). The shade-avoidance syndrome: multiple signals and ecological consequences. Plant Cell Environ. *40*, 2530–2543.

Brockmann, B., Smith, M.W., Zaraisky, A.G., Harrison, K., Okada, K., and Kamiya, Y. (2001). Subcellular localization and targeting of glucocorticoid receptor protein fusions expressed in transgenic *Arabidopsis thaliana*. Plant Cell Physiol. *42*, 942–951.

Casal, J.J., Fankhauser, C., Coupland, G., and Blazquez, M.A. (2004). Signalling for developmental plasticity. Trends Plant Sci. *9*, 309–314.

Cho, S.K., Ben Chaabane, S., Shah, P., Poulsen, C.P., and Yang, S.W. (2014). COP1 E3 ligase protects HYL1 to retain microRNA biogenesis. Nat. Commun. *5*, 5867.

de Felippes, F.F., and Weigel, D. (2010). Transient assays for the analysis of miRNA processing and function. Methods Mol. Biol. *592*, 255–264.

Dong, Z., Han, M.H., and Fedoroff, N. (2008). The RNA-binding proteins HYL1 and SE promote accurate in vitro processing of pri-miRNA by DCL1. Proc. Natl. Acad. Sci. USA *105*, 9970–9975.

Eamens, A.L., Smith, N.A., Curtin, S.J., Wang, M.B., and Waterhouse, P.M. (2009). The *Arabidopsis thaliana* double-stranded RNA binding protein DRB1 directs guide strand selection from microRNA duplexes. RNA *15*, 2219–2235.

Eamens, A.L., Wook Kim, K., and Waterhouse, P.M. (2012). DRB2, DRB3 and DRB5 function in a non-canonical microRNA pathway in *Arabidopsis thaliana*. Plant Signal. Behav. *7*, 1224–1229.

Francisco-Mangilet, A.G., Karlsson, P., Kim, M.H., Eo, H.J., Oh, S.A., Kim, J.H., Kulcheski, F.R., Park, S.K., and Manavella, P.A. (2015). THO2, a core member of the THO/TREX complex, is required for microRNA production in *Arabidopsis*. Plant J. *82*, 1018–1029.

Hellens, R.P., Edwards, E.A., Leyland, N.R., Bean, S., and Mullineaux, P.M. (2000). pGreen: a versatile and flexible binary Ti vector for *Agrobacterium*-mediated plant transformation. Plant Mol. Biol. *42*, 819–832.

Herbert, K.M., Pimienta, G., DeGregorio, S.J., Alexandrov, A., and Steitz, J.A. (2013). Phosphorylation of DGCR8 increases its intracellular stability and induces a progrowth miRNA profile. Cell Rep. *5*, 1070–1081.

Karlsson, P., Christie, M.D., Seymour, D.K., Wang, H., Wang, X., Hagmann, J., Kulcheski, F., and Manavella, P.A. (2015). KH domain protein RCF3 is a tissue-biased regulator of the plant miRNA biogenesis cofactor HYL1. Proc. Natl. Acad. Sci. USA *112*, 14096–14101.

Kurihara, Y., Takashi, Y., and Watanabe, Y. (2006). The interaction between DCL1 and HYL1 is important for efficient and precise processing of pri-miRNA in plant microRNA biogenesis. RNA *12*, 206–212.

Kurihara, Y., and Watanabe, Y. (2004). *Arabidopsis* micro-RNA biogenesis through Dicer-like 1 protein functions. Proc. Natl. Acad. Sci. USA *101*, 12753–12758.

Li, S., Castillo-Gonzalez, C., Yu, B., and Zhang, X. (2017). The functions of plant small RNAs in development and in stress responses. Plant J. *90*, 654–670.

Lu, C., and Fedoroff, N. (2000). A mutation in the *Arabidopsis* HYL1 gene encoding a dsRNA binding protein affects responses to abscisic acid, auxin, and cytokinin. Plant Cell *12*, 2351–2366.

Manavella, P.A., Hagmann, J., Ott, F., Laubinger, S., Franz, M., Macek, B., and Weigel, D. (2012). Fast-forward genetics identifies plant CPL phosphatases as regulators of miRNA processing factor HYL1. Cell *151*, 859–870.

Meng, Y., Shao, C., Wang, H., and Chen, M. (2011). The regulatory activities of plant microRNAs: a more dynamic perspective. Plant Physiol. *157*, 1583–1595.

Pacin, M., Semmoloni, M., Legris, M., Finlayson, S.A., and Casal, J.J. (2016). Convergence of CONSTITUTIVE PHOTOMORPHOGENESIS 1 and PHYTOCHROME INTERACTING FACTOR signalling during shade avoidance. New Phytol. *211*, 967–979.

Paroo, Z., Ye, X., Chen, S., and Liu, Q. (2009). Phosphorylation of the human microRNA-generating complex mediates MAPK/Erk signaling. Cell *139*, 112–122.

Raghuram, B., Sheikh, A.H., Rustagi, Y., and Sinha, A.K. (2015). MicroRNA biogenesis factor DRB1 is a phosphorylation target of mitogen activated protein kinase MPK3 in both rice and *Arabidopsis*. FEBS J. *282*, 521–536.

Reis, R.S., Eamens, A.L., and Waterhouse, P.M. (2015). Missing pieces in the puzzle of plant microRNAs. Trends Plant Sci. *20*, 721–728.

Rodriguez, R.E., Mecchia, M.A., Debernardi, J.M., Schommer, C., Weigel, D., and Palatnik, J.F. (2010). Control of cell proliferation in *Arabidopsis thaliana* by microRNA miR396. Development *137*, 103–112.

Rogers, K., and Chen, X. (2013). Biogenesis, turnover, and mode of action of plant microRNAs. Plant Cell *25*, 2383–2399.

Sarvepalli, K., and Nath, U. (2011). Hyper-activation of the TCP4 transcription factor in *Arabidopsis thaliana* accelerates multiple aspects of plant maturation. Plant J. *67*, 595–607.

Schneider, C.A., Rasband, W.S., and Eliceiri, K.W. (2012). NIH image to ImageJ: 25 years of image analysis. Nat. Methods *9*, 671–675.

Seluzicki, A., Burko, Y., and Chory, J. (2017). Dancing in the dark: darkness as a signal in plants. Plant Cell Environ. *40*, 2487–2501.

Su, C., Li, Z., Cheng, J., Li, L., Zhong, S., Liu, L., Zheng, Y., and Zheng, B. (2017). The protein phosphatase 4 and SMEK1 complex dephosphorylates HYL1 to promote miRNA biogenesis by antagonizing the MAPK cascade in *Arabidopsis*. Dev. Cell *41*, 527–539.e5.

Tomassi, A.H., Gagliardi, D., Cambiagno, D.A., and Manavella, P.A. (2017). Nonradioactive detection of small RNAs using digoxigenin-labeled probes. Methods Mol. Biol. *1640*, 199–210.

Wu, S.H. (2014). Gene expression regulation in photomorphogenesis from the perspective of the central dogma. Annu. Rev. Plant Biol. *65*, 311–333.

Yan, J., Wang, P., Wang, B., Hsu, C.C., Tang, K., Zhang, H., Hou, Y.J., Zhao, Y., Wang, Q., Zhao, C., et al. (2017). The SnRK2 kinases modulate miRNA accumulation in *Arabidopsis*. PLoS Genet. *13*, e1006753.

Yang, S.W., Chen, H.Y., Yang, J., Machida, S., Chua, N.H., and Yuan, Y.A. (2010). Structure of *Arabidopsis* HYPONASTIC LEAVES1 and its molecular implications for miRNA processing. Structure *18*, 594–605.

Yang, X., Ren, W., Zhao, Q., Zhang, P., Wu, F., and He, Y. (2014). Homodimerization of HYL1 ensures the correct selection of cleavage sites in primary miRNA. Nucleic Acids Res. *42*, 12224–12236.

Zhang, Z., Guo, X., Ge, C., Ma, Z., Jiang, M., Li, T., Koiwa, H., Yang, S.W., and Zhang, X. (2017). KETCH1 imports HYL1 to nucleus for miRNA biogenesis in *Arabidopsis*. Proc. Natl. Acad. Sci. USA *114*, 4011–4016.

STAR★METHODS

KEY RESOURCES TABLE

REAGENT or RESOURCE	SOURCE	IDENTIFIER
Antibodies		
Rabbit polyclonal anti-HYL1	Agrisera	Cat#AS06136; RRID:AB_2233541
Rabbit polyclonal anti-SE	Agrisera	Cat#AS09532; RRID:AB_10507110
Rabbit polyclonal anti-ACTIN	Agrisera	Cat#AS132640; RRID:AB_2722610
Rabbit polyclonal anti-H3	Agrisera	Cat# AS10710; RRID:AB_10750790
Goat polyclonal anti-Rabbit IgG, HRP conjugated	Agrisera	Cat#AS09602; RRID:AB_1966902
Anti-Myc	Genscript	Cat#A00704; RRID:AB_914461
Anti-UTPase	Agrisera	Cat#AS05086; RRID:AB_1031827
Mouse monoclonal anti-HIS-HRP	Sigma	Cat#A7058; RRID:AB_258326
Chemicals, Peptides, and Recombinant Proteins		
1-aminocyclopropane-1-carboxylic acid (ACC)	Sigma	Cat#A3903
Jasmonic acid (JA)	Sigma	Cat#J2500
Abscicic acid (ABA)	Sigma	Cat#A1049
Indole-3-acetic acid (IAA)	Sigma	Cat#I2886
Gibberellin (GA3)	Sigma	Cat#48870
6-benzylaminopurine (BAP)	Sigma	Cat#B3408
Cycloheximide (CHX)	MP	Cat#100183
3-(3,4-diclorofenil)-1,1-dimetilurea (DCMU)	DuPont	Cat#
Phos-tag	Wako Chemicals	AAL-107
Dexamethasone (Dex)	Sigma	Cat#D1756
SureBeads Protein-A Magnetic Beads	BioRad	Cat#161-4013
Deposited Data		
Small RNA and mRNA sequencing data	This paper	European Nucleotide Archive (ENA): PRJEB20420
Experimental Models: Organisms/Strains		
Arabidopsis thaliana: Col-0	N/A	N/A
Arabidopsis thaliana: hyl1-2	Arabidopsis Biological Resource Center	SALK_064863
Arabidopsis thaliana: cpl1-7	Manavella et al., 2012	N/A
Arabidopsis thaliana: cpl2-2	Arabidopsis Biological Resource Center	SALK_059753
Arabidopsis thaliana: cpl1-7/cpl2-2	Manavella et al., 2012	N/A
Arabidopsis thaliana: HYL1$^{S>D}$: Pro$_{35S}$::eGFP-HYL1$^{S>D}$ in *hyl1-2*	This Paper	N/A
Arabidopsis thaliana: HYL1$^{S>A}$: Pro$_{35S}$::eGFP-HYL1$^{S>A}$ in *hyl1-2*	This Paper	N/A
Arabidopsis thaliana: HYL1^{S42D}: Pro$_{35S}$::eGFP-HYL1^{S42D} in *hyl1-2*	This Paper	N/A
Arabidopsis thaliana: HYL1^{S159D}: Pro$_{35S}$::eGFP-HYL1^{S159D} in *hyl1-2*	This Paper	N/A
Arabidopsis thaliana: HYL1^{S42A}: Pro$_{35S}$::eGFP-HYL1^{S42A} in *hyl1-2*	This Paper	N/A
Arabidopsis thaliana: HYL1^{S159A}: Pro$_{35S}$::eGFP-HYL1^{S159A} in *hyl1-2*	This Paper	N/A
Arabidopsis thaliana: HYL1^{WT}: Pro$_{35S}$::eGFP-HYL1^{WT} in *hyl1-2*	This Paper	N/A

(*Continued on next page*)

Continued

REAGENT or RESOURCE	SOURCE	IDENTIFIER
Arabidopsis thaliana: HYL1$^{S>D}$: Pro$_{HYL1}$::eGFP-HYL1$^{S>D}$ in *hyl1-2*	This Paper	N/A
Arabidopsis thaliana: HYL1$^{S>A}$: Pro$_{HYL1}$::eGFP-HYL1$^{S>A}$ in *hyl1-2*	This Paper	N/A
Arabidopsis thaliana: HYL1^{S42D}: Pro$_{HYL1}$::eGFP-HYL1^{S42D} in *hyl1-2*	This Paper	N/A
Arabidopsis thaliana: HYL1^{S159D}: Pro$_{HYL1}$::eGFP-HYL1^{S159D} in *hyl1-2*	This Paper	N/A
Arabidopsis thaliana: HYL1^{S42A}: Pro$_{HYL1}$::eGFP-HYL1^{S42A} in *hyl1-2*	This Paper	N/A
Arabidopsis thaliana: HYL1^{S159A}: Pro$_{HYL1}$::eGFP-HYL1^{S159A} in *hyl1-2*	This Paper	N/A
Arabidopsis thaliana: HYL1^{WT}: Pro$_{HYL1}$::eGFP-HYL1^{WT} in *hyl1-2*	This Paper	N/A
Arabidopsis thaliana: HYL1$^{S>A}$: Pro$_{35S}$::HYL1$^{S>A}$ in *hyl1-2*	This Paper	N/A
Arabidopsis thaliana: HYL1^{S42D}: Pro$_{35S}$::HYL1^{S42D} in *hyl1-2*	This Paper	N/A
Arabidopsis thaliana: HYL1^{S159D}: Pro$_{35S}$::HYL1^{S159D} in *hyl1-2*	This Paper	N/A
Arabidopsis thaliana: HYL1^{S42A}: Pro$_{35S}$::HYL1^{S42A} in *hyl1-2*	This Paper	N/A
Arabidopsis thaliana: HYL1^{S159A}: Pro$_{35S}$::HYL1^{S159A} in *hyl1-2*	This Paper	N/A
Arabidopsis thaliana: HYL1^{WT}: Pro$_{35S}$::HYL1^{WT} in *hyl1-2*	This Paper	N/A
Arabidopsis thaliana: HYL1$^{S>A}$: Pro$_{HYL1}$::HYL1$^{S>A}$ in *hyl1-2*	Manavella et al., 2012	N/A
Arabidopsis thaliana: HYL1^{S42D}: Pro$_{HYL1}$::HYL1^{S42D} in *hyl1-2*	This Paper	N/A
Arabidopsis thaliana: HYL1^{S159D}: Pro$_{HYL1}$::HYL1^{S159D} in *hyl1-2*	This Paper	N/A
Arabidopsis thaliana: HYL1^{S42A}: Pro$_{HYL1}$::HYL1^{S42A} in *hyl1-2*	This Paper	N/A
Arabidopsis thaliana: HYL1^{S159A}: Pro$_{HYL1}$::HYL1^{S159A} in *hyl1-2*	Manavella et al., 2012	N/A
Arabidopsis thaliana: HYL1^{WT}: Pro$_{HYL1}$::HYL1^{WT} in *hyl1-2*	This Paper	N/A
Arabidopsis thaliana: HYL1-GR: Pro$_{HYL1}$::HYL1-GR in *hyl1-2*	This Paper	N/A
Arabidopsis thaliana: HYL1-6xMyc: 35S::HYL1-6xMyc in *hyl1-2*	This Paper	N/A
Arabidopsis thaliana: HYL1^{mNES}-6xMyc: 35S::HYL1^{mNES}-6xMyc in *hyl1-2*	This Paper	N/A
Yeast: HYL1: Pro$_{ADH1}$::GAL4AD-HYL1 in Y187	This Paper	N/A
Yeast: HYL1^{S42D}: Pro$_{ADH1}$::GAL4AD-HYL1^{S42D} in Y187	This Paper	N/A
Yeast: HYL1^{S159D}: Pro$_{ADH1}$::GAL4AD-HYL1^{S159D} in Y187	This Paper	N/A
Yeast: HYL1^{S42A}: Pro$_{ADH1}$::GAL4AD-HYL1^{S42A} in Y187	This Paper	N/A
Yeast: HYL1^{S159A}: Pro$_{ADH1}$::GAL4AD-HYL1^{S159A} in Y187	This Paper	N/A
Yeast: HYL1: Pro$_{ADH1}$::GAL4BD-HYL1 in Y187	This Paper	N/A
Yeast: Pro$_{ADH1}$::GAL4BD-SE in Y187	This Paper	N/A
Oligonucleotides		
miRNA sequencing analysis results	This Paper	Table S1
RNA sequencing analysis results	This Paper	Table S2
Probes for small RNA blotting	This Paper	Table S4

(*Continued on next page*)

Continued		
REAGENT or RESOURCE	SOURCE	IDENTIFIER
Primers for qRT-PCR	This Paper	Table S4
Primers for plasmid construction	This Paper	Table S4
Recombinant DNA		
HIS:HYL1	This Paper	Table S3
Software and Algorithms		
ImageJ	NIH	https://imagej.nih.gov/ij/
Trim_galore!	Babraham Bioinformatics	https://www.bioinformatics.babraham.ac.uk/projects/trim_galre/
STAR	GitHub	https://github.com/alexdobin/STAR
Bowtie2	SourceForge	bowtie-bio.sourceforge.net/bowtie2/
TopHat2	CCB - Johns Hopkins University	https://ccb.jhu.edu/software/tophat/
cuffdiff	Trapnell Lab	cole-trapnell-lab.github.io/cufflinks/cuffdiff/
DESeq	Bioconductor	https://bioconductor.org/packages/release/bioc/html/DESeq.htm

CONTACT FOR REAGENT AND RESOURCE SHARING

Further information and requests for resources and reagents should be directed to and will be fulfilled by the Lead Contact, Pablo A. Manavella (pablomanavella@ial.santafe-conicet.gov.ar).

EXPERIMENTAL MODEL AND SUBJECT DETAILS

Plant Material

The *Arabidopsis* (*Arabidopsis thaliana*) ecotype Columbia (Col-0, CS22681), was used in this study. Mutant plants and transgenic lines used in this study are listed in the Key Resources Table. Plants were grown on soil or in plates containing 0.5X Murashige and Skoog Basal Medium (MS) and 0.8% agar at 23°C in 16 hours light/8 hours dark for long day photoperiod.

METHOD DETAILS

Light Conditions

We used three basic protocols to simulate conditions where the plants experienced limited light levels (i) by young etiolated seedlings buried in the soil (etiolated seedlings), (ii) by adult light-grown plants re-buried in the soil (re-burial) and (iii) by adult light-grown plants shaded by neighbor plants (shade). For experiments with etiolated seedlings, seeds were stratified at 4°C for 3 days, exposed to white light for 1 hour to synchronize germination and placed in darkness at 23°C. In a variant of these experiments we exposed seedlings to unilateral blue light because these light conditions are sufficient to initiate phototropic responses but not to achieve full de-etiolation. For re-burial and shade, plants were grown for 10 days under 16 hr white light /8 hr darkness at 23°C. A photosynthetically active radiation (400-700 nm) of 100 μmol m-2 s-1 was provided by fluorescent lamps. Then, the plants were transferred either to darkness (reburial) or under simulated shade. To simulate shade, green filters were applied to reach a fluence rate of 10 μmol m-2s-1 and red/far-red ratio = 0.1, which emulates the light perceived by a plant in nature when located under the canopy of neighbor plants (Pacin et al., 2016). In some experiments these protocols involving limiting light were followed by the transfer of the seedlings to the white light conditions described above to investigate the transitions leading to de-etiolation or the termination of re-burial or shade conditions.

Temperature and Pharmacological Treatments

For abiotic stress treatments, 10-day-old seedlings were subjected to 24 hours of either dark or cold (4°C). When using transgenic plants, and unless specifically stated in the figure, we pooled T2 plants from at least 10 lines of similar expression levels to avoid any bias of a particular individual line. In all experiments whole seedlings, including aerial tissues and roots, were used unless specifically stated. For hormone treatments, 10-day-old seedlings were placed for 12 hours in MS medium containing 30 μM 1-aminocyclopropane-1-carboxylic acid (ACC); 200 μM jasmonic acid (JA); or 100 μM abscicic acid (ABA), indole-3-acetic acid (IAA), gibberellin (GA3) or 6-benzylaminopurine (BAP). For cycloheximide (CHX) and DCMU treatments, 10-day-old seedlings were transferred to darkness for the indicated periods of times and then to MS medium containing 100 μM CHX or 50 μM DCMU two or one hour before seedlings were back to light, respectively. To test transgenic plants expressing HYL1-GR fusions in skotomorphogenesis assays, seeds were germinated in MS plates containing 10 μM dexamethasone or mock solution. When shade avoidance response was evaluated in

HYL1-GR transgenic plants, 15-day-old seedlings grown in long day photoperiod were sprayed with 30 μM dexamethasone or mock solution both 2 days and 2 hours before transferring them to simulated shade.

Plasmid Construction

To create Pro35S::eGFP-HYL1 phosphomimics/WT, Pro35S::HYL1 phosphomimics, ProHYL1::HYL1 S42D and S159A, and ProADH1::GAL4AD-HYL1 phosphomimics constructs, entry vectors harboring previously reported HYL1 phosphomimics [1] were recombined with the destination vectors pFK247, pFK210, pPM415 and pDEST22 (Thermo fisher), respectively. pFK247, pFK210 and pPM415 are pGREEN based vectors (Hellens et al., 2000). To create ProHYL1::eGFP-HYL1 phosphomimics and WT constructs, the eGFP-HYL1 fusions were amplified by PCR with *Pfu* DNA polymerase (Thermo Fisher Scientific), cloned into p-ENTR-D-TOPO (Thermo Fisher Scientific) and then recombined with pPM415. To create ProHYL1::HYL1-GR, HYL1-GR fusion was obtained by overlapping PCR with *Pfu* DNA polymerase (Thermo Fisher Scientific), cloned into p-ENTR-D-TOPO and then recombined with pPM415. See Table S3 for detailed list of constructs and ids, and Table S4 to see the oligonucleotide primers used for cloning. Vectors from the pGREEN series, used for transformation, confer either ammonium glufosinate or kanamycin resistance in plants. All recombination reactions were performed using LR Clonase Enzyme (TermoFisher Scientific).

Plant Transient Transformation

For transient expression, 2-week old N. benthamiana leaves were infiltrated following a standard protocol (de Felippes and Weigel, 2010). Briefly, *Agrobacterium tumefaciens* strain GV3101 harboring the gene of interest on a binary plasmid was grown on Luria-broth (LB) medium containing 100 μg/ml rifampicin, 50 μg/ml kanamycin, 100 μg/ml spectinomycin and 5 μg/ml gentamycin. Fresh culture was centrifuged, and the bacterial pellet was resuspended in infiltration medium (10 mM MgCl2, 10 mM MES pH 5.7, 150 mM acetosyringone). After three hours of incubation at room temperature (21-23°C) and gentle agitation, the volume was adjusted with the infiltration medium to a final optical density of 0.5 at 600 nm. Transiently transformed leaves were analyzed 3 days after infiltration.

RNA Analysis

Total RNA was extracted using TRIZOL reagent (Thermo Fisher Scientific). RNA blots were performed as previously described (Tomassi et al., 2017). Briefly, 1-5 μg of total RNA were resolved in 17% (v/v) polyacrylamide gels under denaturing conditions (7 M urea) and then transferred to HyBond-N+ charged nylon membranes (Amersham) by semidry electroblotting. RNA was covalently fixed to membranes in an UV Crosslinker. Membranes were hybridized over night with DNA oligonucleotide probes labeled with second generation DIG Oligonucleotide 3'-End Labeling Kit (Roche); signal was detected using CSPD ready-to-use solution, by exposure to Amersham hyperfilm ECL (GE Healthcare Life Sciences). For quantitative RT-PCR, 1 μg of total RNA was treated with DNase I (Thermo Fisher Scientific) and cDNA was produced with RevertAid RT Reverse Transcription Kit (Thermo Fisher Scientific). See Table S4 for oligonucleotide primers and probes details.

RNA and Small RNA Sequencing

Small RNA libraries were prepared as indicated by the TruSeq small RNA library prep kit (Illumina). 50 ng of small RNAs purified with the ZR small-RNA PAGE Recovery Kit (Zymo Research) were used as input for the library preparation. mRNA libraries were prepared, using 1 ug of total RNA as input, as described by the TruSeq RNA sample prep V2 guide (Illumina). Small RNA and mRNA libraries size selections were performed using the BluePippin System (SAGE Science). Single-end Illumina sequencing was performed with a HiSeq300 apparatus. Small RNA reads were first processed to remove 3′ adapters using Trim_galore! with the small_rna option (version 0.4.2, https://www.bioinformatics.babraham.ac.uk/projects/trim_galore). Mapping was then performed using STAR (version 2.5.2b) with the following parameters: outFilterScoreMinOverLread 0 outFilterMatchNmin 16 outFilterMatchNminOverLread 0 outFilterMismatchNoverLmax 0.05 seedSearchStartLmax 30 alignIntronMax 1 alignEndsType Local. The reference used was the database hairpin and mature A. thaliana miRNAs from miRBase (release 21), in the latter mature miRNA with identical sequences were collapsed into single miRNAs. Additionally, reads were mapped to the A. thaliana genome and to the miRNA hairpins from miRBase, also with the software STAR. For the differential expression analysis of the miRNAs, only reads mapping to the mature miRNAs with a length of 24 nucleotides or less were considered, and primary alignments of reads mapping to the sense strand were counted (filtering with "samtools view-F 272"). Counts per miRNA were used as input for DESeq in order to perform the differential expression analysis. For this, miRNAs with low expression levels (less than 10 counts in all samples) were discarded and size factors were set according to the total number of reads mapping to the genome for each sample. The mRNA-seq reads were first filtered by mapping them to the 18s ribosomal RNA with Bowtie2 (version 2.2.6). Unmapped reads were then aligned to the A. thaliana genome (TAIR9 release) using Tophat2 (version 2.1.0) with the TAIR10 gene annotation and the following parameters: no-novel-juncs, read-edit-dist 1, read-gap-length 0, max-multihits 1. Finally, differentially expressed genes were found with cuffdiff (version 2.2.1) using the default parameters.

Microscopy

Stably transformed *A. thaliana* plants or *N. benthamiana* leaves, transiently transformed, were placed in dark for one day or kept in long day photoperiod before leaves were imaged on a TCS SP8 confocal microscope (Leica).

FRAP and FLIP Analyses

Arabidopsis protoplasts transiently expressing either HYL1-YFP or NLS-YFP were analyzed. 10 pre-bleaching images were recorded and the average intensity of the 5 last ones was used as the pre-bleaching measurement. Then the nuclei were bleached at maximum laser power for 5 cycles followed by recording of 50 images with 5 seconds intervals. The bleaching reduced the relative fluorescence intensity (RFI) to 40 %. RFI was determined using a slightly modified equation previously described [6]. Briefly, all data were background subtracted and RFI was calculated as (T_0/I_0) X (I_t/T_t) where T_0 is the average total cellular intensity before bleaching, I_0 is the average nuclear intensity before bleaching, I_t is the average nuclear intensity at time t, and T_t is the average total cellular intensity at time t. RFI for each nucleus analyzed was used for curve fitting using GraphPadtm. The GraphPadtm built-in application 'comparison of fits' was applied. Data where the comparison was reported as 'can't calculate' or fit 'ambiguous' were discarded. One component fit yields a single rate constant K and two components fit yields two rate constants K1 and K2 (s^{-1}). For FLIP analysis, *Arabidopsis* protoplasts transiently expressing HYL1-YFP, HYL1^{mNES}-YFP or NLS-YFP were analyzed. A large cytoplasmic area enclosing the nucleus was continuously bleached and the average intensity in the nucleus was recorded with 2.6 seconds intervals for 390 seconds. The analysis commenced after a minimum of 15 bleaching cycles to avoid measuring fluorescent molecules re-entering the nucleus from the cytoplasm. The average intensity in the nucleus was background subtracted and data was analyzed using GraphPadtm. Data from each nucleus was tested either for single or two components in same way as for the FRAP experiments described above. No photobleaching control was calculated from 6 individual cells expressing HYL1-YFP.

Cycloheximide (CHX)-Chase Assay

For the CHX-chase assay, 10-day-old seedlings of WT/HYL1-6xMyc and WT/HYL1^{mNES}-6xMyc transgenic plants were treated with Cycloheximide (0.5 mM) as the indicated time (0, 40, 80, and 120 min) and then samples were mixed with 5× SDS sample buffer for 10 min, and extracts were resolved on 8 to 12% SDS-PAGE after boiling at 100°C.

Cell Fractionation and Size-Exclusion Chromatography Analyses

10-day-old seedlings of Col-0 were homogenized in nuclei isolation buffer (20 mM Tris-HCl (pH 7.4), 25% glycerol, 20 mM KCl, 250 mM sucrose, 2.5 mM MgCl2, 1 mM phenylmethylsulfonyl fluoride and 1 × protease inhibitor cocktail (Roche)). The extracts were filtered through the two layer of miracloth (calbiochem) and centrifuged at 1,000g for 10 min to harvest the supernatant and pellet. The pellet was washed twice with nuclear isolation buffer including 0.2% Triton X-100 to obtain the nuclear fraction, and the supernatant was centrifuged at 27,000g for 30 min to harvest the cytosolic fraction [7]. The nuclear fraction was dissolved in nuclear isolation buffer and sonicated twice for 15 s. Nuclear fraction and cytosolic extracts (1 mg) were passed through a 0.2 μm filter before loading into a Sephadex 200-pg gel filtration column (Hiprep, 16/600; GE Healthcare). Size-exclusion chromatography analysis was performed by AKTA prime plus (GE healthcare). Protein samples were applied to the column, pre-equilibrated with column buffer (50 mM Tris-HCl, pH 7.5, 2 mM EDTA, 1 mM $MgCl_2$, 100 mM NaCl, and 1 mM phenylmethylsulfonyl fluoride) at 0.5 ml/min. Fractions (1.0 mL) were collected and concentrated by Strataclean Resin (Agilent). Samples were mixed with 5x sample buffer and separated by SDS/PAGE.

Protein Analyses

For western blot analysis, proteins were extracted from 300 mg ground tissue with 300 ml ice-cold extraction buffer (50 mM Tris [pH 7.5], 150 mM NaCl, 1 mM EDTA, 10% [v/v] glycerol, 1 mM DTT, 1 mM Pefablock, and one tablet of Complete Protease Inhibitor Cocktail (Roche) per 10 ml of prepared buffer). Proteins were resolved in 8-12% SDS-PAGE gels (running buffer: 25 mM Tris-Base; 192 mM Glycin; 0.1% SDS). Thermo Scientific PageRuler Prestained Protein Ladder was used to determine the molecular weight of the bands and to confirm transfer efficiency. Membranes where split at the ~55 kDa mark the upper part was used to detect HYL1 while the lower part for Actin. Phosphoisoforms were separated in gels with 50 mM Phos-Tag (Wako Chemicals, Neuss, Germany) and 100 mM $MnCl_2$. No EDTA was added to the extraction buffer when the proteins were used for Phos-Tag containing gels; instead, one tablet of PhosStop (ROCHE) per 10 ml of buffer was added. Standard wet tank transfer was used for blotting (blotting buffer: 2.5 mM Tris-Base; 19.2 mM Glycine; 20% (v/v) methanol); just in the case of Phos-tag gels, only 5% methanol was added to the transfer buffer to improve the process. Thermo Scientific PageRuler Prestained Protein Ladder was used only to confirm transfer efficiency, as molecular markers are not functional in Phos-tag gels (manufacturer instructions and Figure S5M). HYL1 isoforms were detected using a polyclonal antibody targeting the *Arabidopsis* protein (dilution 1:10,000) (Agrisera). ACTIN 8 (dilution 1:20,000) (Agrisera), or coomassie blue staining, were used as loading controls. To detect primary antibodies, polyclonal anti-rabbit IgG, HBR conjugated, was used (dilution 1:20,000). Signal was detected using ECL Plus Western Blotting Substrate (Thermo Fisher Scientific). HYL1 isoform identity was confirmed in the Phos-tag gels by including a sample extracted from *hyl1-2* mutants that lack the protein (Figure S5M, Manavella et al., 2012). Yeast two-hybrid assays were performed with the ProQuest Two-Hybrid System (Thermo Fisher Scientific). To reduce autoactivation, different concentrations of 3-AT (3-amino-1,2,4-triazole), added to the selection medium, were assayed.

Cell-Free HYL1 Degradation and Phosphorylation Assay

To test HYL1 degradation in a cell-free system, proteins were extracted using a cell-free degradation buffer (1x PBS, 10mM $MgCl_2$ and 10% glycerol) from 10-day-old seedlings. Purified recombinant HIS-HYL1 (1 μg) were mixed with 10 μg of *cop1-6* extracts and incubated at 30°C for one hour (See Table S3 for description of the recombinant protein constructs). The reaction samples were

separated by 13% SDS-PAGE gel, transferred to a membrane and the recombinant protein was detected with a HIS-HRP antibody (dilution 1:5,000, Sigma, USA). To test HYL1 phosphorylation in a cell-free system, recombinant HIS-HYL1 was purified using Ni-NTA resin from crude extract of E. coli harboring pEX-HYL1 clone (Cho et al., 2014). HIS-HYL1 bound Ni-NTA resin was incubated with phosphorylation buffer (1xPBS, 10 mM $MgCl_2$, 10 mM MG132, 0.5x Protease inhibitor cocktail), [λ-32P] ATP (20 μCi per reaction) and cytoplasmic crude extracts of wild type seedlings (500 μg) for two hours. After reaction, the resin was washed twice with washing buffer (1x PBS) and eluted with Imidazole (100 mM). Samples were resolved in 13% SDS-PAGE and stained by coomassie blue (Sun-Gel Staining Solution, LPS solution, Korea). Phosphorylated proteins were visualized by autoradiography using phospho-imager. Cytoplasmic crude extracts without HIS-HYL1 bound resin were tested as negative control.

RNA Immunoprecipitation Assay

For RNA immunoprecipitation experiments, 1 g of 10-day-old seedlings grown on MS agar plates were collected after UV crosslinking. A 1/5000 dilution of an anti-HYL1 antibody (Agrisera) and SureBeads Protein-A magnetic bead (Bio-Rad) were used to immunoprecipitate protein–RNA complexes. After elution of protein–RNA complexes, RNA and proteins were extracted using TRIZOL reagent (Thermo Fisher Scientific). First-strand cDNA and RT-PCR of the associated RNAs were performed using the RevertAid RT Reverse Transcription Kit and DreamTaq PCR Master Mix (Thermo Fisher Scientific) (Francisco-Mangilet et al., 2015).

QUANTIFICATION AND STATISTICAL ANALYSIS

Quantitative RT-PCR was performed by using at least biological triplicates. All replicates were treated as independent samples for statistical purposes. Averages and SEM were calculated from 2-ΔΔCt values. P-values of less than 0.05 in a t-test with Bonferroni's correction were considered significant. ImageJ (Schneider et al., 2012) was used to analyze seedlings' hypocotyl length, band intensity of western and small RNA blots, and nuclear fluorescence of cells expressing eGFP-HYL1 fusions. Both band intensity and nuclear fluorescence were analyzed as integrated pixel density. To measure hypocotyls length, 4-day-old seedlings grown in MS 0.8% agar were placed on top a black, film used as background and including a scale reference, and scanned at 600 dpi. Hypocotyls lengths were then quantified using ImageJ. For cotyledon and petiole angle measurements, 4- or 15-day-old seedlings respectively, were photographed and analyzed with ImageJ.

DATA AND SOFTWARE AVAILABILITY

The accession number for all data reported in this paper is available at the European Nucleotide Archive (ENA), PRJEB20420.